

# Model Hamiltonian for Topological Insulators

Chao-Xing Liu<sup>1</sup>, Xiao-Liang Qi<sup>2</sup>, HaiJun Zhang<sup>3</sup>, Xi Dai<sup>3</sup>, Zhong Fang<sup>3</sup> and Shou-Cheng Zhang<sup>2</sup>

<sup>1</sup> *Physikalisches Institut (EP3) and Institute for Theoretical Physics and Astrophysics, University of Würzburg, 97074 Würzburg, Germany;*

<sup>2</sup> *Department of Physics, McCullough Building, Stanford University, Stanford, CA 94305-4045; and*

<sup>3</sup> *Beijing National Laboratory for Condensed Matter Physics, and Institute of Physics, Chinese Academy of Sciences, Beijing 100190, China;*

(Dated: November 26, 2024)

In this paper we give the full microscopic derivation of the model Hamiltonian for the three dimensional topological insulators in the  $Bi_2Se_3$  family of materials ( $Bi_2Se_3$ ,  $Bi_2Te_3$  and  $Sb_2Te_3$ ). We first give a physical picture to understand the electronic structure by analyzing atomic orbitals and applying symmetry principles. Subsequently, we give the full microscopic derivation of the model Hamiltonian introduced by Zhang *et al* [1] based both on symmetry principles and the  $\mathbf{k} \cdot \mathbf{p}$  perturbation theory. Two different types of  $k^3$  terms, which break the in-plane full rotation symmetry down to three fold rotation symmetry, are taken into account. Effective Hamiltonian is derived for the topological surface states. Both the bulk and the surface models are investigated in the presence of an external magnetic field, and the associated Landau level structure is presented. For more quantitative fitting to the first principle calculations, we also present a new model Hamiltonian including eight energy bands.

PACS numbers: 71.15.-m, 71.18.+y, 73.20.-r, 73.61.Le

## I. INTRODUCTION

Recently, topological insulators (TI) have been investigated intensively both theoretically and experimentally. [2–4] These insulators are fully gapped in the bulk, but have gapless edge or surface states which are topologically protected by the time reversal symmetry. Topological insulator was first theoretically predicted[5] and experimentally observed[6] in the  $HgTe$  quantum wells. Transport measurements[6, 7] show the existence of the gapless edge channel, which demonstrates that  $HgTe/CdTe$  quantum well is a two-dimensional (2D) TI with quantum spin Hall effect. Later,  $Bi_xSb_{1-x}$  was suggested to be a three-dimensional (3D) TI[8] with topologically non-trivial surface states, which were observed by angle-resolved photoemission spectroscopy (ARPES)[9]. However,  $Bi_xSb_{1-x}$  has a small energy gap, alloy disorder and rather complicated surface states. More recently, new TIs with large bulk gaps  $\sim 0.3eV$  and single Dirac cone surface states have been theoretically predicted for  $Bi_2Te_3$ [1],  $Sb_2Te_3$ [1] and  $Bi_2Se_3$  [1, 10]. ARPES measurement[10, 11] indeed shows the single Dirac cone with linear dispersion around the  $\Gamma$  point in both  $Bi_2Se_3$  and  $Bi_2Te_3$ . Current research on these materials is developing rapidly. [12–30]

For deeper understanding and quantitative predictions of novel phenomena associated with the TIs, it is highly desirable to construct standard models for both 2D and 3D TIs. Bernevig, Hughes and Zhang (BHZ)[5] constructed the model Hamiltonian for the 2D TI in  $HgTe$  quantum wells. This model Hamiltonian demonstrates the basic mechanism of TI behavior through band inversion induced by spin-orbit coupling (SOC). It has been applied successfully for quantitative predictions of the helical edge states and properties under magnetic fields.[31]

Zhang *et al*[1] derived a model Hamiltonian for the 3D TI  $Bi_2Se_3$ ,  $Bi_2Te_3$  and  $Sb_2Te_3$ , and obtained topological surface states consisting of a single Dirac cone. Interestingly, in the thin film limit, the 3D TI model reduces exactly to the 2D TI model by BHZ[32–34]. In this paper, we give the full microscopic derivation of our model Hamiltonian, first by constraining its form by symmetry principles and a careful analysis of the relevant atomic orbitals. Subsequently, we determine the parameters of our model Hamiltonian by a systematic  $\mathbf{k} \cdot \mathbf{p}$  expansion near the  $\Gamma$  point, and comparison with the *ab initio* calculations[1]. Furthermore the higher order  $k^3$  terms neglected in Ref. [1], are also included in the derivation in order to recover the crystal  $C_3$  rotation symmetry[35]. Compared to the symmetry arguments given in Ref.[1], the new derivation given in this paper determines all the parameters of our model Hamiltonian by the wavefunctions from *ab initio* calculation, so that no fitting is required and no ambiguity is introduced. As an application of our model Hamiltonian, we study the bulk and surface Landau level spectra in a magnetic field. The surface Landau levels have  $\sqrt{B}$  field dependence, as is expected from the Dirac-type dispersion of the surface states. The gap of 0th Landau level can be as large as  $50meV$  for  $10T$  magnetic field, which suggests that the topological magneto-electric effect[36, 37] can be observable at such energy scales. Furthermore, we propose a more quantitative description of the  $Bi_2Se_3$  family of TIs by going beyond the four bands and present a new model Hamiltonian with eight bands. Recently, our model Hamiltonian has been applied successfully for understand a number of experiments, including the STM study of the topological surface states[14, 20], STM study of the surface bound states[30], STM study of the quasi-particle interference[14, 20, 38], crossover from 3D to 2D topological insulators[21, 32–34], and the Landau level of

the topological surface states[22, 23].

The paper is organized as follows. In sec. II we first present the lattice structure and the symmetry properties of  $\text{Bi}_2\text{Se}_3$  crystal. Then we turn to the electronic band structure and discuss about the atomic orbital picture, which is helpful to capture the essential physics in the long wave length limit. Keeping such atomic orbital picture in mind, we investigate in detail the properties of the bands near Fermi surface based on the symmetry argument in sec. III. Furthermore, our model Hamiltonian for the conduction and valence bands is derived from the theory of invariants. In sec. IV, we re-derive our model Hamiltonian from the  $\mathbf{k} \cdot \mathbf{p}$  theory and determine its parameters by more fundamental matrix elements of the momentum operator in the  $\mathbf{k} \cdot \mathbf{p}$  theory. As an application of our model Hamiltonian, the surface state Hamiltonian and the Landau levels for both the bulk and surface states are calculated in Sec. V and Sec. VI respectively. In Sec. VII, the quantitative limitation of our model Hamiltonian with four-bands is discussed and a new model Hamiltonian is proposed to describe the  $\text{Bi}_2\text{Se}_3$  type of materials more quantitatively. In Sec. VIII we provide a brief discussion and conclusion.

## II. CRYSTAL STRUCTURE, ATOMIC ORBITALS AND SYMMETRY

In this section we will describe the crystal structure of  $\text{Bi}_2\text{Se}_3$  family of materials, and discuss the relevant atomic orbitals and the discrete symmetries. A large portion of the content of this section is already discussed in Ref. [1], but we feel that it is helpful to present the more complete version of this discussion here, to make this paper self-contained. The crystal structure of  $\text{Bi}_2\text{Se}_3$  is rhombohedral with the space group  $D_{3d}^5 (R\bar{3}m)$ . As shown in Fig. 1 (a), the crystal has layered structure stacked along z-direction with five atoms (two *Bi* atoms and three *Se* atoms) in one unit cell, including two equivalent *Se* atoms (*Se1* and *Se1'*), two equivalent *Bi* atoms (*Bi1* and *Bi1'*) and one *Se* atom (*Se2*) which is inequivalent to the *Se1* and *Se1'* atoms. Therefore five atomic layers can be viewed as one unit, which is usually called a quintuple layer. Each atomic layer forms a triangle lattice, which has three possible positions, denoted as A, B and C, as shown in Fig.1 (c). Along the z-direction, the triangle layers are stacked in the order  $A-B-C-A-B-C-\dots$ . We note that the primitive lattice vector  $\vec{t}_i$  ( $i = 1, 2, 3$ ) is not directed along the z direction. For example, in one quintuple layer, the *Se2* atoms occupy the A sites; in the next quintuple layer, the *Se2* atoms do not occupy the A sites but rather the C or B sites. Our coordinate is set as the following: the origin point is set at the *Se2* site; z direction is set perpendicular to the atomic layer, x direction is taken along the binary axis with the two fold rotation symmetry and y direction is taken along the bisectrix axis, which is the crossing line of the reflection plane and the *Se2* atomic

layer plane. The Brillouin Zone (BZ) of this lattice structure is shown in Fig. 1 (b). This crystal structure has the following discrete symmetries:

- *Three fold rotation symmetry  $R_3$  along z direction.*  $R_3$  can be generated by the following transformation:  $x \rightarrow x \cos \theta - y \sin \theta$ ,  $y \rightarrow x \sin \theta + y \cos \theta$  and  $z \rightarrow z$ , where  $\theta = \frac{2\pi}{3}$ .
- *Two fold rotation symmetry  $R_2$  along x direction.*  $R_2$  corresponds to the following transformation:  $\text{Se2} \rightarrow \text{Se2}$ ,  $\text{Bi1} \rightarrow \text{Bi1}'$ ,  $\text{Se1} \rightarrow \text{Se1}'$ ;  $z \rightarrow -z$ ,  $x \rightarrow x$ ,  $y \rightarrow -y$ . For this symmetry operation, we find that *Bi1* (*Se1*) and *Bi1'* (*Se1'*) layers interchange their positions.
- *Inversion  $P$ .*  $P$ :  $\text{Se2} \rightarrow \text{Se2}$ ,  $\text{Bi1} \rightarrow \text{Bi1}'$ ,  $\text{Se1} \rightarrow \text{Se1}'$ ;  $z \rightarrow -z$ ,  $x \rightarrow -x$ ,  $y \rightarrow -y$ . The *Se2* site is the inversion center of this lattice structure, hence we set *Se2* as the origin point. Under inversion operation, *Bi1* (*Se1*) is changed to *Bi1'* (*Se1'*).
- *Time reversal symmetry  $T$ .* Time reversal operation is given by  $T = \Theta K$ , where  $\Theta = i\sigma_2$  and  $K$  is the complex conjugate operator. Here  $\sigma_{1,2,3}$  are the Pauli matrices for spin.

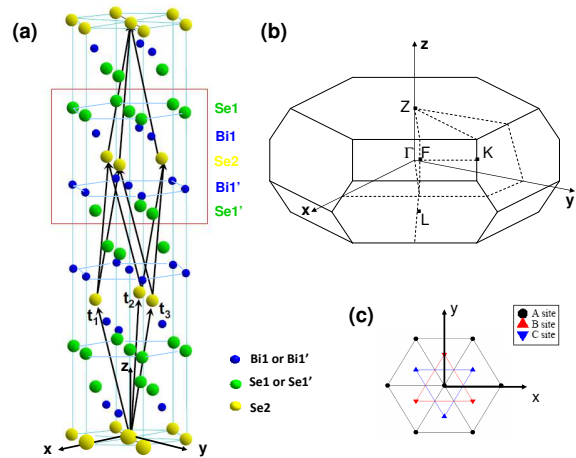


FIG. 1: (a) The crystal structure of  $\text{Bi}_2\text{Se}_3$ .  $\vec{t}_{1,2,3}$  is the primitive lattice vector, given by  $\vec{t}_1 = (\sqrt{3}a/3, 0, c/3)$ ,  $\vec{t}_2 = (-\sqrt{3}a/6, a/2, c/3)$ ,  $\vec{t}_3 = (-\sqrt{3}a/6, -a/2, c/3)$ ; where  $a$  is the lattice constant in the x-y plane and  $c$  is the lattice constant along the z direction. The quintuple layer is shown in the red box with  $\text{Se1} - \text{Bi1} - \text{Se2} - \text{Bi1}' - \text{Se1}'$ .  $\text{Se1}$  ( $\text{Bi1}$ ) and  $\text{Se1}'$  ( $\text{Bi1}'$ ) are equivalent. (b) Brillouin Zone of  $\text{Bi}_2\text{Se}_3$ . (c) The in-plane triangle lattice has three possible position A, B and C.

In order to get a physical picture of the band structure of  $\text{Bi}_2\text{Se}_3$ , we start from the atomic orbitals of *Bi* and *Se*. The electron configuration of *Bi* is  $6s^26p^3$  and that of *Se* is  $4s^24p^4$ . The outmost shells for both *Bi* and *Se* are p-orbital, therefore it is natural to consider only p-orbitals

of *Bi* and *Se* and neglect other orbitals. As discussed above,  $Bi_2Se_3$  has a layered structure. The chemical bonding is very strong within one quintuple layer but the two neighboring quintuple layers are only coupled by the van der Waals force. Therefore it is reasonable for us to first focus on one quintuple layer. Within one quintuple layer there are 5 atoms in one unit cell and each atom has three orbitals ( $p_x$ ,  $p_y$  and  $p_z$ ), therefore totally there are 15 orbitals. The spin is neglected first and will be discussed later when we introduce SOC into the system. We denote these orbitals as  $|\Lambda, \alpha\rangle$  with  $\Lambda = Bi1, Bi1', Se1, Se2, Se1'$  and  $\alpha = p_x, p_y, p_z$ . As shown in Fig.1 (a), the *Se2* atomic layer stays in the middle of the quintuple layer and is sandwiched by two *Bi* layers (*Bi1* and *Bi1'*), while two *Se* layers (*Se1* and *Se1'*) are located at the outermost. Since all the *Se* layers are separated by *Bi* layers, the strongest coupling in this system is the coupling between *Bi* layers and *Se* layers. Such coupling causes level repulsion, so that the *Bi* energy levels are pushed up and form new hybridized states  $|B_\alpha\rangle$  and  $|B'_\alpha\rangle$  while the *Se* energy levels are pushed down and yield three states  $|S_\alpha\rangle$ ,  $|S'_\alpha\rangle$  and  $|S0_\alpha\rangle$ , as shown in Fig.2 (I). Since the system has inversion symmetry, it is convenient to combine these orbitals to form the bonding and anti-bonding states with the definite parity, which are given by

$$\begin{aligned} |P1^\pm, \alpha\rangle &= \frac{1}{\sqrt{2}}(|B_\alpha\rangle \mp |B'_\alpha\rangle) \\ |P2^\pm, \alpha\rangle &= \frac{1}{\sqrt{2}}(|S_\alpha\rangle \mp |S'_\alpha\rangle) \end{aligned} \quad (1)$$

with the upper index denoting the parity and  $\alpha = p_x, p_y, p_z$ . When the coupling between  $|B_\alpha(S_\alpha)\rangle$  and  $|B'_\alpha(S'_\alpha)\rangle$  is taken into account, the bonding and anti-bonding states are split, with the anti-bonding state having higher energy than the bonding state. Therefore as shown in Fig.2 (II), the states  $|P1^+, \alpha\rangle$  and  $|P2^-, \alpha\rangle$  are found to be near the Fermi surface, hence we focus on  $|P1^+, \alpha\rangle$  and  $|P2^-, \alpha\rangle$  ( $\alpha = p_x, p_y, p_z$ ) and neglect the other states. Furthermore the crystal has layered structure, so the  $z$  direction is different from the  $x$  or  $y$  directions in the atomic plane. Thus there is an energy splitting between  $p_z$  and  $p_{x,y}$  orbitals for both  $P1^+$  and  $P2^-$  states. We find that  $|P1^+, p_{x,y}\rangle$  orbitals have higher energy than  $|P1^+, p_z\rangle$ , while  $|P2^-, p_{x,y}\rangle$  orbitals have lower energy than  $|P2^-, p_z\rangle$ . Consequently, the conduction band mainly consists of  $|P1^+, p_z\rangle$  while the valence band is dominated by the  $|P2^-, p_z\rangle$  orbital before SOC is considered, as shown in Fig.2 (III).

Next we include SOC effect in the above atomic picture. The states  $|P1^+, \alpha, \sigma\rangle$  and  $|P2^-, \alpha, \sigma\rangle$  are all double degenerate, with one more index  $\sigma = \uparrow, \downarrow$  to denote spin. The atomic SOC Hamiltonian is given by  $\hat{H}_{so} = \lambda \mathbf{s} \cdot \mathbf{L}$  with  $\lambda = \frac{1}{2m_0^2 c^2} \frac{1}{r} \frac{\partial U}{\partial r}$  depending on the detail potential  $U$  of atoms, which couples orbital angular momentum to spin. It is convenient to transform the  $p_x$  and  $p_y$  orbitals to  $p_\pm$  with definite orbital angular mo-

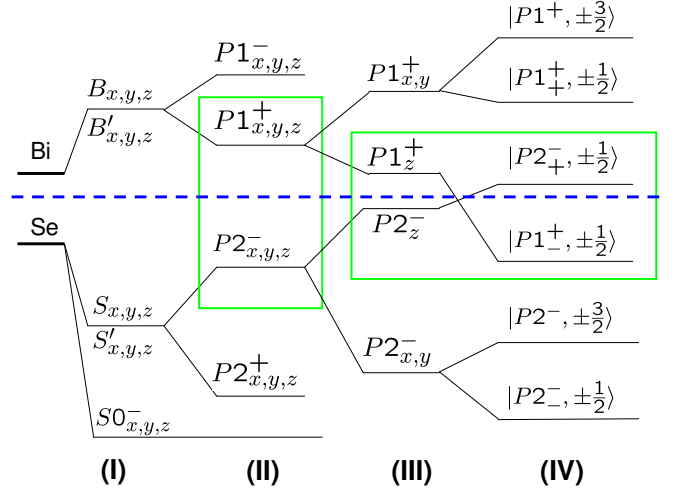


FIG. 2: Schematic picture of the origin of the band structure of  $Bi_2Se_3$ . Starting from the atomic orbitals of *Bi* and *Se*, the following four steps are required to understand the band structure: (I) the hybridization of *Bi* orbitals and *Se* orbitals, (II) the formation of the bonding and antibonding states due to the inversion symmetry, (III) the crystal field splitting and (IV) the influence of the SOC.

mentum:

$$|\Lambda, p_+, \sigma\rangle = -\frac{1}{\sqrt{2}}(|\Lambda, p_x, \sigma\rangle + i|\Lambda, p_y, \sigma\rangle), \quad (2)$$

$$|\Lambda, p_-, \sigma\rangle = \frac{1}{\sqrt{2}}(|\Lambda, p_x, \sigma\rangle - i|\Lambda, p_y, \sigma\rangle), \quad (3)$$

where  $\Lambda = P1^+, P2^-$ . Within this basis, the atomic SOC Hamiltonian is given by

$$\begin{aligned} \langle \Lambda, p_+, \uparrow | H_{so} | \Lambda, p_+, \uparrow \rangle &= \langle \Lambda, p_-, \downarrow | H_{so} | \Lambda, p_-, \downarrow \rangle \equiv \frac{\lambda_\Lambda}{2} \\ \langle \Lambda, p_+, \downarrow | H_{so} | \Lambda, p_+, \downarrow \rangle &= \langle \Lambda, p_-, \uparrow | H_{so} | \Lambda, p_-, \uparrow \rangle \equiv -\frac{\lambda_\Lambda}{2} \\ \langle \Lambda, p_+, \downarrow | H_{so} | \Lambda, p_z, \uparrow \rangle &= \langle \Lambda, p_-, \uparrow | H_{so} | \Lambda, p_z, \downarrow \rangle \equiv \frac{\lambda_\Lambda}{\sqrt{2}} \\ \langle \Lambda, p_z, \uparrow (\downarrow) | H_{so} | \Lambda, p_z, \uparrow (\downarrow) \rangle &= 0. \end{aligned} \quad (4)$$

Here the value of  $\lambda_\Lambda$  is a linear combination of the SOC coefficient for *Bi* and *Se*, depending on how much the orbitals of *Bi* and *Se* are mixed into the state  $|\Lambda\rangle$ . The sign of  $\lambda_\Lambda$  is always positive for  $\Lambda = P1^+, P2^-$  since the potential is always attractive for atoms. As we see, since the total angular momentum along the  $z$  direction is still conserved, hybridization only occurs between  $|\Lambda, p_z, \uparrow\rangle$  ( $|\Lambda, p_z, \downarrow\rangle$ ) and  $|\Lambda, p_+, \downarrow\rangle$  ( $|\Lambda, p_-, \uparrow\rangle$ ). After taking into account SOC, the new eigen-states are given by

$$|\Lambda, \frac{3}{2}\rangle = |\Lambda, p_+, \uparrow\rangle \quad (5)$$

$$|\Lambda, -\frac{3}{2}\rangle = |\Lambda, p_-, \downarrow\rangle \quad (6)$$

$$|\Lambda_+, \frac{1}{2}\rangle = u_+^\Lambda |\Lambda, p_z, \uparrow\rangle + v_+^\Lambda |\Lambda, p_+, \downarrow\rangle \quad (7)$$

$$|\Lambda_-, \frac{1}{2}\rangle = u_-^\Lambda |\Lambda, p_z, \uparrow\rangle + v_-^\Lambda |\Lambda, p_+, \downarrow\rangle \quad (8)$$

$$|\Lambda_+, -\frac{1}{2}\rangle = (u_+^\Lambda)^* |\Lambda, p_z, \downarrow\rangle + (v_+^\Lambda)^* |\Lambda, p_-, \uparrow\rangle \quad (9)$$

$$|\Lambda_-, -\frac{1}{2}\rangle = (u_-^\Lambda)^* |\Lambda, p_z, \downarrow\rangle + (v_-^\Lambda)^* |\Lambda, p_-, \uparrow\rangle \quad (10)$$

with the eigen-energies  $E_{3/2}^\Lambda$  and  $E_{1/2}^{\Lambda\pm}$  (each is double degenerate) and  $u, v$  obtained by solving the following  $2 \times 2$  Hamiltonian

$$\hat{H} = \begin{pmatrix} E_{\Lambda,x} - \lambda_\Lambda/2 & \lambda_\Lambda/\sqrt{2} \\ \lambda_\Lambda/\sqrt{2} & E_{\Lambda,z} \end{pmatrix}. \quad (11)$$

For the above eigen-states (5)~(10), all the information about SOC is included in the coefficient  $u$  and  $v$ , which are given by

$$\begin{pmatrix} u_\pm^\Lambda \\ v_\pm^\Lambda \end{pmatrix} = \frac{1}{N_\pm} \begin{pmatrix} \Delta E_\Lambda \pm \sqrt{(\Delta E_\Lambda)^2 + \frac{\lambda_\Lambda^2}{2}} \\ \lambda_\Lambda/\sqrt{2} \end{pmatrix} \quad (12)$$

explicitly, where  $N_\pm = \lambda_\Lambda^2 + 2\Delta E_\Lambda^2 \pm 2\Delta E_\Lambda \sqrt{\Delta E_\Lambda^2 + \lambda_\Lambda^2/2}$  and  $\Delta E_\Lambda = \frac{E_{\Lambda,x} - E_{\Lambda,z} - \lambda_\Lambda/2}{2}$ . The energy splitting between the  $p_{x(y)}$  orbital and the  $p_z$  orbital due to the crystal field is larger than the energy scale of SOC and  $\Delta E_\Lambda$  is dominated by  $E_{\Lambda,x} - E_{\Lambda,z}$ . Now as we see, the SOC couples  $|\Lambda, p_z, \uparrow\rangle$  ( $|\Lambda, p_z, \downarrow\rangle$ ) to  $|\Lambda, p_+, \downarrow\rangle$  ( $|\Lambda, p_-, \uparrow\rangle$ ) so that it induces the level repulsion between these two states. Consequently,  $|P1^\pm, \pm\frac{1}{2}\rangle$  is pushed down while  $|P2^\pm, \pm\frac{1}{2}\rangle$  is pushed up, which yields the level crossing between these two pairs of states, when the SOC is strong enough, as shown in Fig.2 (IV). Since these two pairs of states have the opposite parity, their crossing leads to a *band inversion*, similar to the case in the *HgTe* quantum wells[5]. This is the key signature of the topological insulator phase in *Bi<sub>2</sub>Se<sub>3</sub>* family of materials[1]. Therefore in the following we will focus on these four states and regard the other states as the perturbation.

### III. MODEL HAMILTONIAN DERIVED FROM SYMMETRY PRINCIPLES

From the discussion of the atomic orbitals in the last section, we obtain an intuitive physical picture of the band structure of *Bi<sub>2</sub>Se<sub>3</sub>*. Compared with the *ab initio* calculation, we can denote the bands near Fermi surface by  $|\Lambda^\pm, \alpha\rangle$  where  $\Lambda = P1_\pm, P2_\pm$  and  $\alpha = \pm\frac{1}{2}, \pm\frac{3}{2}$ , as shown in Fig 3. Roughly, these states mainly consist of the bonding or anti-bonding states of the p-orbitals of *Bi* or *Se* atoms. However, other orbitals such as s-orbitals of *Bi* and *Se* will also mix into these states. To identify each band without any ambiguity, it is necessary to relate each band with the representation of the crystal symmetry. At  $\Gamma$  point, each state should belong to an

irreducible representation of the crystal symmetry group and the hybridization between orbitals preserve the symmetry properties. Therefore, a suitable method to identify each band is to use the symmetry of the crystal. In this section, we will first identify each band according to the irreducible representation of the crystal group  $D_{3d}^5$  and then try to derive our model Hamiltonian just from symmetry principles.

First let's consider the states without spin, which are denoted as  $|\Lambda^\pm, \alpha\rangle$  with  $\Lambda = P1, P2$  and  $\alpha = p_x, p_y, p_z$ . The crystal of *Bi<sub>2</sub>Se<sub>3</sub>* belongs to the group  $D_{3d}^5$  with the character table given in table (I) of Appendix A[39]. Since the crystal is inversion symmetric, each representation has a definite parity eigenvalue. For each parity, there are two one-dimensional representations  $\tilde{\Gamma}_1^\pm$  and  $\tilde{\Gamma}_2^\pm$  and one two-dimensional representation  $\tilde{\Gamma}_3^\pm$ , where the upper index denotes the parity (+ for even and - for odd). According to the wave functions constructed from the simple atomic orbital picture, we can determine the transformation property of the wave functions under the generators  $R_3, R_2$  and  $P$  of the point group. For example, let's look at the operation  $R_2$  on the state  $|P1^+, p_x\rangle = \frac{1}{\sqrt{2}}(|B_x\rangle - |B'_x\rangle)$ . The  $R_2$  rotation does not change the  $p_x$  orbital, however it changes the position of *Bi1* (*Se1*) and *Bi1'* (*Se1'*) and correspondingly changes  $|B\rangle$  to  $|B'\rangle$ , thus we should have  $R_2|P1^+, p_x\rangle = -|P1^+, p_x\rangle$ . Similiar argument can be applied to other states and finally the transformation of the states under the crystal symmetry operation is listed as follows.

- *Three fold rotation symmetry  $R_3$* :  $|\Lambda^\pm, p_x\rangle \rightarrow \cos\theta|\Lambda^\pm, p_x\rangle - \sin\theta|\Lambda^\pm, p_y\rangle$ ,  $|\Lambda^\pm, p_y\rangle \rightarrow \sin\theta|\Lambda^\pm, p_x\rangle + \cos\theta|\Lambda^\pm, p_y\rangle$  and  $|\Lambda^\pm, p_z\rangle \rightarrow |\Lambda^\pm, p_z\rangle$ , with  $\theta = \frac{2\pi}{3}$ .
- *Two fold rotation symmetry  $R_2$* :  $|\Lambda^\pm, p_x\rangle \rightarrow \mp|\Lambda^\pm, p_x\rangle$ ,  $|\Lambda^\pm, p_y\rangle \rightarrow \pm|\Lambda^\pm, p_y\rangle$ ,  $|\Lambda^\pm, p_z\rangle \rightarrow \pm|\Lambda^\pm, p_z\rangle$ .
- *Inversion  $P$* :  $|\Lambda^\pm, \alpha\rangle \rightarrow \pm|\Lambda^\pm, \alpha\rangle$ ,  $\alpha = p_x, p_y, p_z$ .

Here  $\Lambda = P1_\pm, P2_\pm$ . According to the above transformation, we find that  $|\Lambda^{+(-)}, p_x\rangle$  and  $|\Lambda^{+(-)}, p_y\rangle$  belong to the  $\tilde{\Gamma}_3^{+(-)}$  representation.  $|\Lambda^+, p_z\rangle$  belongs to  $\tilde{\Gamma}_1^+$  representation and  $|\Lambda^-, p_z\rangle$  belongs to  $\tilde{\Gamma}_2^-$  representation.

To take into account spin, we introduce the spinor representation  $\tilde{\Gamma}_6^\pm$ , which changes its sign under the rotation  $\mathcal{C} = 2\pi$ . The double group of  $D_{3d}^5$  can be constructed by the direct product of  $\tilde{\Gamma}_{1,2,3}^\pm$  and  $\tilde{\Gamma}_6^\pm$ . As shown in (A1) ~ (A3), we find that  $\tilde{\Gamma}_3^\pm \otimes \tilde{\Gamma}_6^\pm$  will give two new one-dimensional representations  $\tilde{\Gamma}_4^\pm$  and  $\tilde{\Gamma}_5^\pm$ , which are conjugate to each other. The character table of the double group for  $D_{3d}^5$  is given in table (II) of Appendix A[39]. With SOC, the eigen-states in (5) ~ (6) can also be analysed by the decomposition of direct production. From (A2) and (A3), the direct product of  $\tilde{\Gamma}_6^\pm$  and  $\tilde{\Gamma}_{1,2}^\pm$  always gives  $\tilde{\Gamma}_6^\pm$  representation, therefore  $|\Lambda^+, \pm\frac{1}{2}\rangle$  with  $\Lambda = P1, P2$  should belong to  $\tilde{\Gamma}_6^+$  representation while  $|\Lambda^-, \pm\frac{1}{2}\rangle$  should belong to  $\tilde{\Gamma}_6^-$  representation.

The states  $|\Lambda^\pm, \pm 3/2\rangle$  originate from the combination of  $|\Lambda, p_{x,y}\rangle$  and spin. According to (A1), it is expected that  $|\Lambda^\pm, \pm 3/2\rangle$  should be a combination of  $\tilde{\Gamma}_4^\pm$  and  $\tilde{\Gamma}_5^\pm$  representations. Indeed by carefully inspecting the transformation behavior under the operation  $R_2$  and  $R_3$ , we find that

$$|\Lambda^\pm, \tilde{\Gamma}_4\rangle = \frac{1}{\sqrt{2}}(|\Lambda^\pm, 3/2\rangle + |\Lambda^\pm, -3/2\rangle) \quad (13)$$

belongs to the  $\tilde{\Gamma}_4^\pm$  representation, while

$$|\Lambda^\pm, \tilde{\Gamma}_5\rangle = \frac{1}{\sqrt{2}}(|\Lambda^\pm, 3/2\rangle - |\Lambda^\pm, -3/2\rangle) \quad (14)$$

belongs to the  $\tilde{\Gamma}_5^\pm$  representation. The above results can also be worked out by considering the forms of the transformation for the states (5) ~ (6), which are given by

- *Three fold rotation symmetry  $R_3$* :  $|\Lambda, \pm \frac{1}{2}\rangle \rightarrow e^{\pm i\frac{2\pi}{3}}|\Lambda, \pm \frac{1}{2}\rangle$ ,  $|\Lambda, \pm \frac{3}{2}\rangle \rightarrow -|\Lambda, \pm \frac{3}{2}\rangle$ , where  $\Lambda = P1_\pm^\pm, P2_\pm^\pm$ .
- *Two fold rotation symmetry  $R_2$* :  $|\Lambda^+, \pm \frac{1}{2}\rangle \rightarrow i|\Lambda^+, \mp \frac{1}{2}\rangle$ ,  $|\Lambda^-, \pm \frac{1}{2}\rangle \rightarrow -i|\Lambda^-, \mp \frac{1}{2}\rangle$ ,  $|\Lambda^+, \pm \frac{3}{2}\rangle \rightarrow i|\Lambda^+, \mp \frac{3}{2}\rangle$ ,  $|\Lambda^-, \pm \frac{3}{2}\rangle \rightarrow -i|\Lambda^-, \mp \frac{3}{2}\rangle$ , with  $\Lambda = P1_\pm, P2_\pm$ .
- *Inversion  $P$* :  $|\Lambda^\pm, \alpha\rangle \rightarrow \pm|\Lambda^\pm, \alpha\rangle$ , with  $\Lambda = P1_\pm, P2_\pm$  and  $\alpha = \pm\frac{3}{2}, \pm\frac{1}{2}$ .

It is instructive to compare the present case with the more common semiconductor crystal structures, such as diamond or zinc-blende structure. In that case, the coupling between p orbitals and the spin usually gives the four-dimensional  $\tilde{\Gamma}_8$  and the two-dimensional  $\tilde{\Gamma}_7$  representation. In the present case, due to the lower symmetry of the crystal structure, the  $\tilde{\Gamma}_7$  representation is the same as the  $\tilde{\Gamma}_6$  representation while the  $\tilde{\Gamma}_8$  representation is reduced to two one-dimensional representations  $\tilde{\Gamma}_4$  and  $\tilde{\Gamma}_5$  and one two-dimensional representation  $\tilde{\Gamma}_6$ . In Fig 3, the representation of the bands near the Fermi surface is given.

Next we derive our model Hamiltonian to describe the low energy physics of  $Bi_2Se_3$  just based on the symmetry of the wave function at  $\Gamma$  point. As described above, near the Fermi surface the conduction band and valence band are determined by the four states  $|P1_\pm^\pm, \pm \frac{1}{2}\rangle$  and  $|P2_\mp^\pm, \pm \frac{1}{2}\rangle$ , belonging to the  $\tilde{\Gamma}_6^+$  and  $\tilde{\Gamma}_6^-$  representation. Therefore the minimum model Hamiltonian for  $Bi_2Se_3$  should be written with these four states as the basis. Generally, any  $4 \times 4$  Hamiltonian can be expanded with Dirac  $\Gamma$  matrices as

$$\hat{H}_{eff} = \epsilon(\mathbf{k})\mathbf{I} + \sum_i d_i(\mathbf{k})\Gamma_i + \sum_{ij} d_{ij}(\mathbf{k})\Gamma_{ij} \quad (15)$$

where  $\mathbf{I}$  is the  $4 \times 4$  identity matrix,  $\Gamma_i$  ( $i = 1 \dots 5$ ) denote the five Dirac  $\Gamma$  matrices satisfying  $\{\Gamma_i, \Gamma_j\} = 2\delta_{ij}$ ,

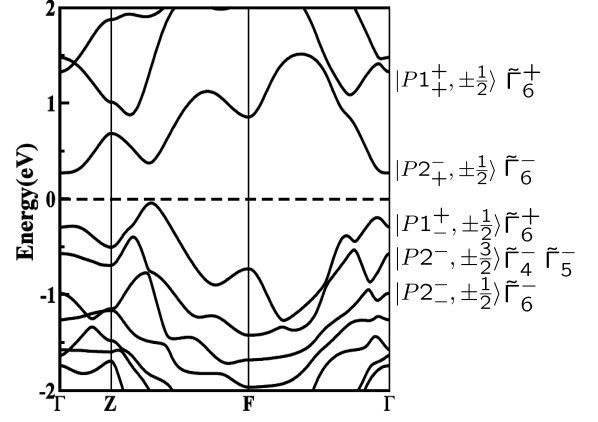


FIG. 3: The band structure of  $Bi_2Se_3$  is obtained from *ab initio* calculation, and the bands near Fermi surface is identified with  $|\Lambda^\pm, \alpha\rangle$ .  $\Lambda = P1_\pm, P2_\pm$  and  $\alpha = \pm\frac{1}{2}, \pm\frac{3}{2}$ . The corresponding irreducible representation is also given.

and the ten anti-commutators of  $\Gamma$  matrices are given by  $\Gamma_{ij} = [\Gamma_i, \Gamma_j]/2i$ .  $\epsilon(\mathbf{k})$ ,  $d_i(\mathbf{k})$  and  $d_{ij}(\mathbf{k})$  can be expanded by the powers of the momentum  $\mathbf{k}$ . The construction of  $\Gamma$  is given in Appendix B. Now let's assume the above Hamiltonian is written in the basis  $|P1_\pm^\pm, \pm \frac{1}{2}\rangle$ ,  $|P2_\mp^\pm, \pm \frac{1}{2}\rangle$ ,  $|P1_\mp^\pm, -\frac{1}{2}\rangle$  and  $|P2_\mp^\pm, -\frac{1}{2}\rangle$ . Then according to the transformation of the states under the symmetry operation discussed above, we can construct the transformation matrices as follows.

- *Time reversal symmetry*:  $T = \Theta K$ , where  $\Theta = i\sigma_2 \otimes 1$  and  $K$  is the complex conjugate operator.
- *Three fold rotation symmetry operation*:  $R_3 = e^{i\frac{\Pi}{2}\theta}$  with  $\Pi = \sigma_3 \otimes 1$  and  $\theta = \frac{2\pi}{3}$ .
- *Two fold rotation symmetry operation*:  $R_2 = i\sigma_1 \otimes \tau_3$ .
- *Inversion*:  $P = 1 \otimes \tau_3$ .

In the above,  $\sigma$  acts in the spin basis and  $\tau$  acts in the basis of  $P1^+$  and  $P2^-$  sub-bands. According to the above transformation matrices, we can obtain the irreducible representation of each  $\Gamma$  matrix, details of which are derived in Appendix B. The invariance of the Hamiltonian requires that the function  $d_i(\mathbf{k})$  ( $d_{ij}(\mathbf{k})$ ) should have the same behavior to the corresponding  $\Gamma_i$  ( $\Gamma_{ij}$ ) matrix under the symmetry operation, which means that they should belong to the same representation of the crystal point group. In the table III of the Appendix B, we list the representation for both the  $\Gamma$  matrices and the polynomials of  $\mathbf{k}$ , and also their transformation properties under the time reversal operation. Since we hope to preserve both time reversal symmetry and crystal symmetry, we must choose the  $\Gamma$  matrices and polynomials of  $\mathbf{k}$  with the same representation. For example,  $\Gamma_1$  and  $\Gamma_2$  carry the representation  $\tilde{\Gamma}_3^-$  and are odd under time reversal,

and so are  $k_x$  and  $k_y$ . Therefore they can together form an invariant term for Hamiltonian. Finally, up to  $O(k^3)$ , our model Hamiltonian yields

$$\begin{aligned} H'_{eff} &= H'_0 + H'_3 \\ H'_0 &= \epsilon_{\mathbf{k}} + \mathcal{M}(\mathbf{k})\Gamma_5 + \mathcal{B}(k_z)\Gamma_4 k_z \\ &+ \mathcal{A}(k_{\parallel})(\Gamma_1 k_y - \Gamma_2 k_x) \\ H'_3 &= R_1\Gamma_3(k_x^3 - 3k_x k_y^2) + R_2\Gamma_4(3k_x^2 k_y - k_y^3) \end{aligned} \quad (16)$$

where  $\epsilon_{\mathbf{k}} = C_0 + C_1 k_z^2 + C_2 k_{\parallel}^2$ , and  $\mathcal{M}(\mathbf{k}) = M_0 + M_1 k_z^2 + M_2 k_{\parallel}^2$  and  $\mathcal{A}(k_{\parallel}) = A_0 + A_2 k_{\parallel}^2$  and  $\mathcal{B}(k_z) = B_0 + B_2 k_z^2$  and  $k_{\parallel}^2 = k_x^2 + k_y^2$ .  $H'_0$  keeps the in-plane rotation symmetry along  $z$  direction, while  $H'_3$  breaks the in-plane rotation symmetry down to three fold rotation symmetry. In the following, we find the bulk  $H'_3$  term will also lead to the correction to the effective surface Hamiltonian, which has been studied in Ref. [35].

The above Hamiltonian is the same to that presented by Zhang *et al* in the Ref. [1], which can be shown by performing the transformation

$$U_1 = \begin{pmatrix} 1 & 0 & 0 & 0 \\ 0 & -i & 0 & 0 \\ 0 & 0 & 1 & 0 \\ 0 & 0 & 0 & i \end{pmatrix}, \quad (18)$$

and the Hamiltonian is transformed into

$$\begin{aligned} H_{eff} &= H_0 + H_3 \\ H_0 &= U_1 H'_0 U_1^\dagger = \epsilon_{\mathbf{k}} + \\ &\begin{pmatrix} \mathcal{M}(\mathbf{k}) & \mathcal{B}(k_z)k_z & 0 & \mathcal{A}(k_{\parallel})k_- \\ \mathcal{B}(k_z)k_z & -\mathcal{M}(\mathbf{k}) & \mathcal{A}(k_{\parallel})k_- & 0 \\ 0 & \mathcal{A}(k_{\parallel})k_+ & \mathcal{M}(\mathbf{k}) & -\mathcal{B}(k_z)k_z \\ \mathcal{A}(k_{\parallel})k_+ & 0 & -\mathcal{B}(k_z)k_z & -\mathcal{M}(\mathbf{k}) \end{pmatrix} \\ H_3 &= U_1 H'_3 U_1^\dagger = \frac{R_1(k_+^3 + k_-^3)}{2} \begin{pmatrix} 0 & i & 0 & 0 \\ -i & 0 & 0 & 0 \\ 0 & 0 & 0 & i \\ 0 & 0 & -i & 0 \end{pmatrix} \\ &+ \frac{R_2(k_+^3 - k_-^3)}{2} \begin{pmatrix} 0 & -i & 0 & 0 \\ -i & 0 & 0 & 0 \\ 0 & 0 & 0 & i \\ 0 & 0 & i & 0 \end{pmatrix} \end{aligned} \quad (19)$$

Now we can see that  $H_0$  is nearly the same to the model Hamiltonian (1) in Ref. [1], except the  $A_2$  term and  $B_2$  term, which represent the high order correction to the Fermi velocity  $A_0$  and  $B_0$ . Since such correction is not important near  $\Gamma$  point, we will neglect these two terms in the following. Derivation of our model Hamiltonian (19) and (20) from the symmetry principles is the central result of this section.

#### IV. MODEL HAMILTONIAN DERIVED FROM THE $\mathbf{k} \cdot \mathbf{p}$ PERTURBATION THEORY

Up to now we have obtained our model Hamiltonian from the symmetry principles, or the theory of

invariants[40]. In this section, we will derive the model Hamiltonian through another way,  $\mathbf{k} \cdot \mathbf{p}$  theory, and connect the parameters of the model Hamiltonian to the more fundamental matrix elements of momentum in  $\mathbf{k} \cdot \mathbf{p}$  theory.

The basic idea of  $\mathbf{k} \cdot \mathbf{p}$  theory is to use the wave function at  $\Gamma$  point in BZ as the zeroth-order wave function and treat

$$\hat{H}' = \frac{\hbar}{m_0} \mathbf{k} \cdot \mathbf{p} \quad (21)$$

as a perturbation, where  $\mathbf{p} = -i\hbar\partial_{\mathbf{r}}$  is the momentum operator acting on the zeroth-order wave function and the crystal momentum  $\mathbf{k}$  is regarded as a small parameter during the perturbation procedure. The model Hamiltonian is expanded by the powers of  $k$ . With the perturbation formalism (C18)  $\sim$  (C21), we can project the system into the subspace spanned by the four states  $|P1_{-}^{\pm}, 1/2\rangle \equiv |1\rangle$ ,  $|P2_{+}^{\pm}, 1/2\rangle \equiv |2\rangle$ ,  $|P1_{+}^{\pm}, -1/2\rangle \equiv |3\rangle$  and  $|P2_{+}^{\pm}, -1/2\rangle \equiv |4\rangle$ , which are used as the basis of our model Hamiltonian. All the other states are treated in the perturbation procedure and the details are given in Appendix C. The obtained model Hamiltonian will depend on a series of matrix elements of momentum  $\langle \Lambda_1, \alpha | \mathbf{p} | \Lambda_2, \beta \rangle$ , which can be simplified due the symmetry of the crystal. For example, due to the existence of the inversion symmetry, all the states at  $\Gamma$  point have definite parity eigenvalues. Since the momentum  $\mathbf{p}$  has odd parity, the matrix elements of momentum between two states with the same parity always vanish. The wave function at the  $\Gamma$  point can be obtained through *ab initio* calculation, consequently all these matrix elements can be calculated. With these matrix elements, we apply the perturbation formalism (C18)  $\sim$  (C21) to the system and recover our model Hamiltonian (19) and (20). The parameters of our model Hamiltonian  $C_0, C_1, C_2, M_0, M_1, M_2, A_0, B_0, R_1$  and  $R_2$  can be expressed as the function of the parameters  $P_{\Lambda_1, \Lambda_2}, Q_{\Lambda_1, \Lambda_2}, M_{\Lambda_1, \Lambda_2}, N_{\Lambda_1, \Lambda_2}, R_{\Lambda_1, \Lambda_2}$  and  $S_{\Lambda_1, \Lambda_2}$  through (C22)  $\sim$  (C31) in the Appendix C. With these expressions, we can numerically calculate the values of the parameters of our model Hamiltonian, which is listed in table IV. We note that the parameters given here are different from those in Ref. [1] and [41], where the parameters are determined by fitting to the energy dispersion, which has some ambiguity. In the present method, since we directly calculate the matrix elements of momentum from microscopic wave functions, there is no ambiguity.

The key result of this section are the parameters of our model Hamiltonian, given in table IV. The fitted energy dispersions for  $Bi_2Se_3$ ,  $Bi_2Te_3$  and  $Sb_2Te_3$  are plotted in Fig 4. It is shown that our model Hamiltonian is valid in the regime  $k_{x,z} < 0.04\text{\AA}^{-1}$ . However the maximum of the valence band for  $Bi_2Se_3$  and  $Bi_2Te_3$  stays away from  $\Gamma$  point, at about  $k_x \approx 0.07\text{\AA}^{-1}$ , therefore we need to keep in mind that there may be some discrepancies when we try to use our model Hamiltonian to describe  $Bi_2Se_3$  quantitatively. Since our model Hamiltonian with four

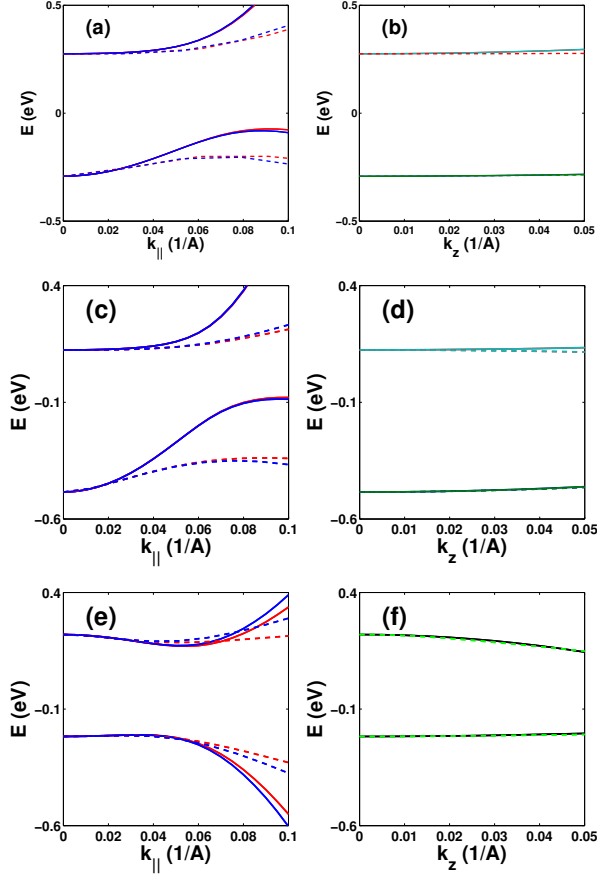


FIG. 4: The energy dispersion obtained from our model Hamiltonian with four bands (solid line) is compared with that from *ab initio* calculation (dashed line). Here (a) and (b) is for  $Bi_2Se_3$ , (c) and (d) is for  $Bi_2Te_3$ , while (e) and (f) is for  $Sb_2Te_3$ . In (a), (c) and (e), the red line represents the dispersion along  $k_x$  direction while the blue line is for  $k_y$  direction.

bands already captures the salient features of the band dispersion, especially the inverted band structure, in the following two sections, we still stay in the framework of our model Hamiltonian to discuss the topological surface states and the Landau levels in the magnetic field. Then in the last section, we will extend our model Hamiltonian to include eight bands, in order to describe these materials more quantitatively.

## V. SURFACE STATES

An important physical consequence of the non-trivial topology is the existence of topological surface states. In this section, we would like to study the surface state and its effective Hamiltonian based on our model Hamiltonian derived above with open boundary condition.

Consider our model Hamiltonian (17) defined on the half space given by  $z > 0$ . We can divide our model

Hamiltonian into two parts

$$\hat{H} = \tilde{H}_0 + \tilde{H}_1 \quad (22)$$

$$\tilde{H}_0 = \tilde{\epsilon}(k_z) + \tilde{M}(k_z)\Gamma_5 + B_0\Gamma_4k_z \quad (23)$$

$$\begin{aligned} \tilde{H}_1 = & C_2k_{\parallel}^2 + M_2k_{\parallel}^2\Gamma_5 \\ & + A_0(\Gamma_1k_y - \Gamma_2k_x) + H_3. \end{aligned} \quad (24)$$

where  $\tilde{\epsilon}(k_z) = C_0 + C_1k_z^2$  and  $\tilde{M}(k_z) = M_0 + M_1k_z^2$ . All  $k_z$  dependent terms are included in  $\tilde{H}_0$ . We replace  $k_z$  by  $-i\partial_z$ , and obtain the eigen-value equation

$$\tilde{H}_0(k_z \rightarrow -i\partial_z)\Psi(z) = E\Psi(z) \quad (25)$$

Since  $\Gamma_4 = 1 \otimes \tau_2$  and  $\Gamma_5 = 1 \otimes \tau_3$  are both block-diagonal, the Hamiltonian  $\tilde{H}_0$  is also block-diagonal and the eigenstates have the form

$$\Psi_{\uparrow}(z) = \begin{pmatrix} \psi_0 \\ \mathbf{0} \end{pmatrix} \quad \Psi_{\downarrow}(z) = \begin{pmatrix} \mathbf{0} \\ \psi_0 \end{pmatrix}, \quad (26)$$

where  $\mathbf{0}$  is a two-component zero vector.  $\Psi_{\uparrow}(z)$  is related to  $\Psi_{\downarrow}(z)$  by time-reversal operation. To obtain the surface states, the wave function  $\psi_0(z)$  should be localized at the surface and satisfies the eigen-equation

$$\left( \tilde{\epsilon}(-i\partial_z) + \tilde{M}(-i\partial_z)\tau_3 - iB_0\tau_2\partial_z \right) \psi_0(z) = E\psi_0(z) \quad (27)$$

which has been solved analytically for the open boundary condition with different methods.[31, 32, 41–43] Here in order to show the existence of the surface states and to find the region where the surface states exist, we would like to briefly review the derivation for the explicit form of the surface states by neglecting the  $\tilde{\epsilon}$  for simplicity[31].

After neglecting the  $\tilde{\epsilon}$  term, the eigen equation (27) has the particle hole symmetry, therefore we would like to expect a special surface states with  $E = 0$  can exist. With the wave function ansatz  $\psi_0 = \phi e^{\lambda z}$ , the above equation can be simplified as

$$(M_0 - M_1\lambda^2) \tau_1 \phi = B_0\lambda\phi. \quad (28)$$

It is obvious that the two-component wave function  $\phi$  should be the eigen-state of Pauli matrix  $\tau_1$ . Let's define  $\tau_1\phi_{\pm} = \pm\phi_{\pm}$ , then the equation (28) is simplified to a quadratic equation for  $\lambda$ . Another important observation is that if  $\lambda$  is a solution for  $\phi_+$ , then  $-\lambda$  is the solution for  $\phi_-$ . Consequently, the generic wave function is given by

$$\psi_0(z) = (ae^{\lambda_1 z} + be^{\lambda_2 z})\phi_+ + (ce^{-\lambda_1 z} + de^{-\lambda_2 z})\phi_-, \quad (29)$$

where  $\lambda_{1,2}$  satisfy

$$\lambda_{1,2} = \frac{1}{2M_1} \left( -B_0 \pm \sqrt{4M_0M_1 + B_0^2} \right). \quad (30)$$

Similar to the Ref. [31], the open boundary condition  $\psi(0) = 0$ , together with the normalizability of the wave

function in the region  $z > 0$ , leads to the existence condition of the surface states,  $\Re\lambda_{1,2} < 0$  ( $c = d = 0$ ) or  $\Re\lambda_{1,2} > 0$  ( $a = b = 0$ ), which can only be satisfied with the band inversion condition  $M_0M_1 < 0$ . Furthermore, it is easy to show that when  $B_0/M_1 > 0$ ,  $\Re\lambda_{1,2} < 0$ , while  $B_0/M_1 < 0$ ,  $\Re\lambda_{1,2} > 0$ , thus the wave function for the surface states at  $\Gamma$  point is given by

$$\psi_0(m) = \begin{cases} a(e^{\lambda_1 z} - e^{\lambda_2 z})\phi_+ & B_0/M_1 > 0 \\ c(e^{-\lambda_1 z} - e^{-\lambda_2 z})\phi_- & B_0/M_1 < 0 \end{cases}. \quad (31)$$

We emphasize here the sign change of  $B_0/M_1$  will change the spin basis of the surface states, which will be the key point to determine the helicity of the Dirac Hamiltonian for the topological surface states. Another important quantity of the surface states is the decaying length, which can be defined as  $l_c = \max\left\{\frac{1}{|\Re(\lambda_{1,2})|}\right\}$ , given by

$$l_c = \begin{cases} \Re\left(\frac{B_0 + \sqrt{4M_0M_1 + B_0^2}}{2M_0}\right) & B_0 > 0, M_1 < 0 \\ \Re\left(\frac{B_0 - \sqrt{4M_0M_1 + B_0^2}}{2M_0}\right) & B_0 < 0, M_1 > 0 \\ \Re\left(-\frac{B_0 + \sqrt{4M_0M_1 + B_0^2}}{2M_0}\right) & B_0 > 0, M_1 > 0 \\ \Re\left(-\frac{B_0 - \sqrt{4M_0M_1 + B_0^2}}{2M_0}\right) & B_0 < 0, M_1 < 0 \end{cases}, \quad (32)$$

where  $\Re$  takes the real part.

In the above, we take a simple tight-binding model to show the existence condition and the form of the wave function for the surface states, which can help us to understand the underlining physics qualitatively, but not quantitatively. In the realistic materials, the detail form of  $\psi_0$  will depend on the material detail, such as the boundary condition or the detail parameters, however the form of the wave function (26) remains valid. Therefore in the following, we just simply treat  $\psi_0$  by some parameters. On the sub-space  $\Psi = [\Psi_\uparrow, \Psi_\downarrow]$ , we find that

$$\begin{aligned} \langle \Psi | \Gamma_1 | \Psi \rangle &= \alpha_1 \sigma_x, & \langle \Psi | \Gamma_2 | \Psi \rangle &= \alpha_1 \sigma_y, \\ \langle \Psi | \Gamma_3 | \Psi \rangle &= \alpha_1 \sigma_z, & \langle \Psi | \Gamma_4 | \Psi \rangle &= 0, \\ \langle \Psi | \Gamma_5 | \Psi \rangle &= \alpha_3, \end{aligned} \quad (33)$$

with  $\alpha_1 \equiv \langle \psi_0 | \tau_1 | \psi_0 \rangle$  and  $\alpha_3 \equiv \langle \psi_0 | \tau_3 | \psi_0 \rangle$ . With these expressions, the effective Hamiltonian of the surface states  $\Psi$  is given by[1]

$$\begin{aligned} H_{sur} &= \tilde{C}_0 + \tilde{C}_2 k_{\parallel}^2 + \tilde{A}(\sigma_x k_y - \sigma_y k_x) + \tilde{R}(k_+^3 + k_-^3)\sigma_z \\ &= (C_0 + \alpha_3 M_0) + (C_2 + \alpha_3 M_2)k_{\parallel}^2 + A_0 \alpha_1 (\sigma_x k_y - \sigma_y k_x) \\ &\quad + \frac{R_1 \alpha_1}{2} (k_+^3 + k_-^3)\sigma_z \end{aligned} \quad (34)$$

with  $k_{\pm} = k_x \pm ik_y = k_{\parallel} e^{\pm i\theta}$ . The  $k^3$  terms have also been found in Ref. [35]. In the following numerical calculation, the coefficient  $\alpha_1$  and  $\alpha_3$  are treated as two fitting parameters to the experiment, given by  $\alpha_1 = \frac{\tilde{A}_{exp}}{A_0} = 0.99$  and  $\alpha_3 = \frac{\tilde{C}_{exp} - C_0}{M_0} = -0.15$ , where  $\tilde{A}_{exp} = 3.29eV \cdot \text{\AA}$

comes from the Fermi velocity of the surfaces states and  $\tilde{C}_{exp} = 0.035eV$  comes from the position of the surface Dirac points[10]. Further we need to check the spin operators in this system. Again we use the wave function from *ab initio* calculation and project the spin operator into the subspace spanned by the four basis states. After we obtain the spin operators for our model Hamiltonian, we can use the eigen wave function (26) to project the spin operator into the surface states subspace. Finally we find that  $\langle \Psi | S_x | \Psi \rangle = S_{x0} \sigma_x$ ,  $\langle \Psi | S_y | \Psi \rangle = S_{y0} \sigma_y$  and  $\langle \Psi | S_z | \Psi \rangle = S_{z0} \sigma_z$  with  $S_{x(y,z)0}$  to be some constants. This indicates that  $\sigma$  matrix in our model Hamiltonian (34) is proportional to the real spin.

The derivation of the surface Hamiltonian (34) is the central result of this section. In the limit  $k \rightarrow 0$ , the linear term in Hamiltonian (34) will be dominant, then the surface states show the linear dispersion with helical spin texture, which has the opposite direction for the conduction and valence band, as shown in Fig.5 (a). Such type of spin texture is similar to one of the fermi surfaces in the usual 2D electron gas with Rashba SOC[40, 44], which can be simply understood from the fact that the inversion symmetry is broken near the surface. The helical spin texture has also been calculated from *ab initio* method[45] and already observed in the pioneering spin-resolved APRES measurement[18]. From (34), the helicity of the spin texture is determined by the sign of the coefficient  $A = A_0 \alpha_1$ , where  $\alpha_1 \equiv \langle \psi_0 | \tau_1 | \psi_0 \rangle$  is related to the spin basis of the surface states (31). Therefore the helicity is determined by the relative sign of  $A_0$  and  $B_0/M_1$ . Furthermore, due to the inversion condition  $M_1 M_0 < 0$ , the sign of  $M_1$  is already determined by the gap  $M_0$ . Consequently, within our model Hamiltonian the helicity of the spin texture is given by the relative sign of the coefficients of two types of linear terms,  $A_0$  and  $B_0$ .

To further explore the origin of the helicity of the spin texture in the atomic levels, we relate the coefficients  $A_0$  and  $B_0$  to the atomic SOC by using the expression (7)~(10), as

$$\begin{aligned} A_0 &= \frac{\hbar}{2m_0} \langle P1_+^+, \frac{1}{2}|p_+|P2_+^-, -\frac{1}{2} \rangle \\ &= \frac{\hbar}{2m_0} \left[ \left( u_-^{P1^+} v_+^{P2^-} \right)^* \langle P1^+, p_z | p_+ | P2^-, p_- \rangle \right. \\ &\quad \left. + \left( v_-^{P1^+} u_+^{P2^-} \right)^* \langle P1^+, p_+ | p_+ | P2^-, p_z \rangle \right] \end{aligned} \quad (35)$$

$$\begin{aligned} B_0 &= \frac{\hbar}{m_0} \langle P1_z^+, p_z | p_z | P2^-, p_z \rangle \\ &= \frac{\hbar}{m_0} \left[ \left( u_-^{P1^+} \right)^* u_+^{P2^-} \langle P1^+, p_z | p_z | P2^-, p_z \rangle \right. \\ &\quad \left. + \left( v_-^{P1^+} \right)^* v_+^{P2^-} \langle P1^+, p_+ | p_z | P2^-, p_+ \rangle \right]. \end{aligned} \quad (36)$$

Here  $|\Lambda, \alpha\rangle$  ( $\Lambda = P1^+, P2^-$  and  $\alpha = p_x, p_y, p_z$ ) are the atomic orbitals without any SOC and all the dependence of SOC are included in the coefficient  $u^\Lambda$  and  $v^\Lambda$ . From (12), we find that for  $u^{\Lambda_1} v^{\Lambda_2}$  it is proportional to  $\lambda_{\Lambda_1}$  (or  $\lambda_{\Lambda_2}$ ), which indicates that  $A_0$  depends on the sign of the

atomic SOC, while it is only possible for  $(u^{\Lambda_1})^* u^{\Lambda_2}$  and  $(v^{\Lambda_1})^* v^{\Lambda_2}$  to be independent of  $\lambda_{\Lambda_{1,2}}$  or be proportional to  $\lambda_{\Lambda_1} \lambda_{\Lambda_2}$ , thus the sign of  $B_0$  will not depend on the atomic SOC. Finally, we conclude that the helicity of the spin texture is originally related to the atomic SOC.

In the above, we have shown how the linear term determines the spin texture of the surface states, which can also be affected by the quadratic term and cubic term in the effective Hamiltonian (34). We solve the eigenvalue problems of the whole effective Hamiltonian and obtain the eigen-energy and eigen states as

$$E_{\pm} = \tilde{C}_0 + \tilde{C}_2 k_{\parallel}^2 \pm \sqrt{\tilde{A}^2 k_{\parallel}^2 + 4\tilde{R}^2 k^6 \cos^2 3\theta} \quad (37)$$

$$\psi_{\pm} = \frac{1}{\sqrt{N}} \begin{pmatrix} \tilde{A}(k_y + ik_x) \\ d_{\pm} - \tilde{R}(k_+^3 + k_-^3) \end{pmatrix} \quad (38)$$

with  $d_{\pm} = \pm \sqrt{\tilde{A}^2 k_{\parallel}^2 + 4\tilde{R}^2 k^6 \cos^2 3\theta}$  and  $N = \tilde{A}^2 k^2 + (\sqrt{\tilde{A}^2 k^2 + 4\tilde{R}^2 k^6 \cos^2 3\theta} - 2\tilde{R}k^3 \cos 3\theta)^2$ . Consequently the spin polarization in  $k$  space is given by

$$\langle \psi_+ | \sigma_x | \psi_+ \rangle = \frac{2\tilde{A}k_y}{N} (d_+ - 2\tilde{R}k^3 \cos 3\theta) \quad (39)$$

$$\langle \psi_+ | \sigma_y | \psi_+ \rangle = -\frac{2\tilde{A}k_x}{N} (d_+ - 2\tilde{R}k^3 \cos 3\theta) \quad (40)$$

$$\langle \psi_+ | \sigma_z | \psi_+ \rangle = \frac{4\tilde{R}k^3 \cos 3\theta}{N} (d_+ - 2\tilde{R}k^3 \cos 3\theta) \quad (41)$$

which is plotted in Fig 5 (b). In the limit  $k \rightarrow 0$ , the spin polarization almost lies in the  $xy$  plane, which is due to the linear term and has been discussed in the above. When  $k$  is increased, the  $k$ -cubic term comes into play, which will not only induce the hexagonal warping of the constant energy contours[35] but also yield  $z$  direction spin polarization, similar to the situation in  $Bi_xSb_{1-x}$  studied by *ab initio* calculation[46].

## VI. MAGNETIC FIELD AND LANDAU LEVEL

In this section, we study the Landau level problem for both the bulk states and the surface states, which is important for predicting or understanding many properties of the system in a magnetic field, such as the SdH oscillation, surface quantum Hall effect and magneto-optics. In this regards, our model Hamiltonian has the unique advantage, since the magnetic field effect cannot be incorporated in *ab initio* calculations. For the realistic finite sample, the bulk Landau levels will always coexist with the surface Landau levels, thus both the two types of Landau levels need to be taken into account. For simplicity, we solve the bulk Landau level for an infinite sample and the surface Landau level for the semi-infinite sample. The mixing effect between bulk and surface Landau levels is neglected here.

For the bulk state, there are two types of contribution from the magnetic field, the orbital effect and the Zeeman effect. The orbital effect can be included by Peierls

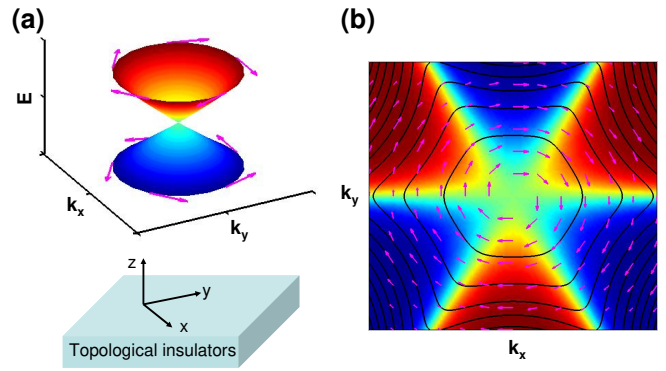


FIG. 5: (a) Spin texture of the surface states near  $\Gamma$  point. For conduction band, the helicity is left handed while for valence band, it is right handed. (b) Spin texture of the conduction band of the surface states in the momentum space. The arrow represents the  $x$ - $y$  planar spin polarization while the color indicates the  $z$  component of the spin polarization. Here red is for spin up while blue is for spin down. The black line gives the constant energy contours.

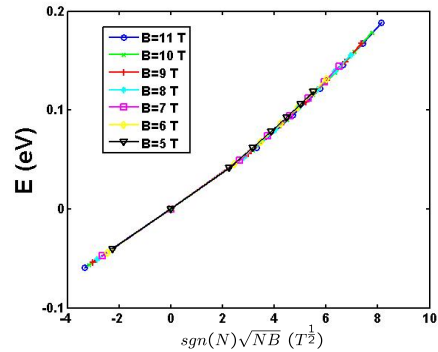


FIG. 6: The energy of the Landau level versus  $\text{sgn}(N)\sqrt{NB}$  where  $N$  is the Landau level index and  $B$  is the magnetic field.

substitution[47]  $\mathbf{k} \rightarrow \pi = \mathbf{k} + \frac{e}{\hbar} \mathbf{A}$  with  $\mathbf{A} = (0, B_z x, 0)$  for magnetic field along  $z$ -direction. We introduce the annihilation and creation operators  $a = \frac{l_c}{\sqrt{2}} \pi_-$  and  $a^\dagger = \frac{l_c}{\sqrt{2}} \pi_+$  with  $l_c = \sqrt{\frac{\hbar}{eB_z}}$  for the harmonic oscillator function  $\varphi_n$ .  $a$  and  $a^\dagger$  satisfy  $a\varphi_N = \sqrt{N}\varphi_{N-1}$ ,  $a^\dagger\varphi_N = \sqrt{N+1}\varphi_{N+1}$  and  $[a, a^\dagger] = 1$ . With the operators  $a$  and  $a^\dagger$ , the Hamiltonian (19) is written as

$$\hat{H}_{0B} = \tilde{\epsilon} + \begin{pmatrix} \tilde{\mathcal{M}} & B_0 k_z & 0 & A_0 \frac{\sqrt{2}}{l_c} a \\ B_0 k_z & -\tilde{\mathcal{M}} & A_0 \frac{\sqrt{2}}{l_c} a & 0 \\ 0 & A_0 \frac{\sqrt{2}}{l_c} a^\dagger & \tilde{\mathcal{M}} & -B_0 k_z \\ A_0 \frac{\sqrt{2}}{l_c} a^\dagger & 0 & -B_0 k_z & -\tilde{\mathcal{M}} \end{pmatrix} \quad (42)$$

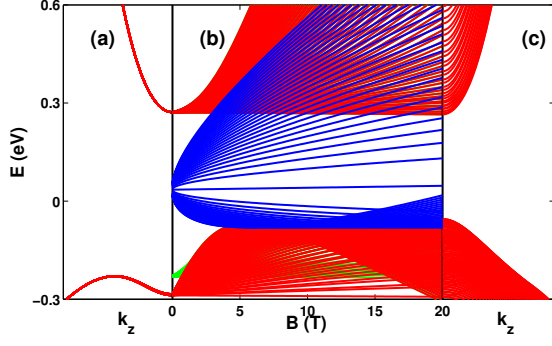


FIG. 7: The Landau levels in the magnetic field for both the bulk states (red lines) and the surface states (blue lines) are shown in (b). Also the dispersion along z direction at (a)  $B = 0T$  and (c)  $B = 20T$  is plotted.

where  $\tilde{\epsilon}(k_z, a^\dagger a) = C_0 + C_1 k_z^2 + \frac{2C_2}{l_c^2} (a^\dagger a + \frac{1}{2})$  and  $\tilde{M}(k_z, a^\dagger a) = M_0 + M_1 k_z^2 + \frac{2M_2}{l_c^2} (a^\dagger a + \frac{1}{2})$ . The  $k^3$  term, which breaks the in-plane rotation symmetry, is neglected here, therefore the wave function should have the form of  $\Psi_N = [f_1^N \varphi_{N-1}, f_2^N \varphi_{N-1}, f_3^N \varphi_N, f_4^N \varphi_N]^T$ . With such wave function ansatz, the Hamiltonian is transformed to

$$\hat{H}_{0B}(k_z, N) = \begin{pmatrix} \tilde{M}_{N-1}^+ & B_0 k_z & 0 & A_0 \frac{\sqrt{2N}}{l_c} \\ B_0 k_z & \tilde{M}_{N-1}^- & A_0 \frac{\sqrt{2N}}{l_c} & 0 \\ 0 & A_0 \frac{\sqrt{2N}}{l_c} & \tilde{M}_N^+ & -B_0 k_z \\ A_0 \frac{\sqrt{2N}}{l_c} & 0 & -B_0 k_z & -\tilde{M}_N^- \end{pmatrix} \quad (43)$$

with  $\tilde{M}_N^+ = \tilde{\epsilon}(k_z, N) + \tilde{\epsilon}(k_z, N)$  and  $\tilde{M}_N^- = \tilde{\epsilon}(k_z, N) - \tilde{\epsilon}(k_z, N)$ .

To consider the Zeeman splitting, we need to further calculate the effective g-factor[40, 48]. The effective Zeeman type coupling can also written down for our model Hamiltonian by symmetry principles. By a quick inspection of the table (III), we find that the following terms

$$\begin{aligned} \hat{H}_Z &= \tilde{g}_{z1} \Gamma_{12} B_z + \tilde{g}_{z2} \Gamma_{34} B_z \\ &+ \tilde{g}_{xy1} \begin{pmatrix} \Gamma_{23} & \Gamma_{31} \end{pmatrix} \begin{pmatrix} \cos \phi_1 & \sin \phi_1 \\ -\sin \phi_1 & \cos \phi_1 \end{pmatrix} \begin{pmatrix} B_x \\ B_y \end{pmatrix} \\ &+ \tilde{g}_{xy2} \begin{pmatrix} \Gamma_{14} & \Gamma_{24} \end{pmatrix} \begin{pmatrix} \cos \phi_2 & \sin \phi_2 \\ -\sin \phi_2 & \cos \phi_2 \end{pmatrix} \begin{pmatrix} B_x \\ B_y \end{pmatrix} \end{aligned} \quad (44)$$

are possible couplings to the magnetic field. Again  $\phi_1$  and  $\phi_2$  are phase factors which need to be determined from other methods, and here we take  $\phi_1 = \phi_2 = 0$  to coincide with the results from the  $\mathbf{k} \cdot \mathbf{p}$  method, and explicitly (44) can be written as

$$\hat{H}_Z = \frac{\mu_B}{2} \begin{pmatrix} g_{1z} B_z & 0 & g_{1p} B_- & 0 \\ 0 & g_{2z} B_z & 0 & g_{2p} B_- \\ g_{1p} B_+ & 0 & -g_{1z} B_z & 0 \\ 0 & g_{2p} B_+ & 0 & -g_{2z} B_z \end{pmatrix} \quad (45)$$

with  $\mu_B = \frac{e\hbar}{2m_0}$ , and  $\tilde{g}_{xy1} + \tilde{g}_{xy2} = \frac{\mu_B}{2} g_{1p}$ ,  $\tilde{g}_{xy1} - \tilde{g}_{xy2} = \frac{\mu_B}{2} g_{2p}$ ,  $\tilde{g}_{z1} + \tilde{g}_{z2} = \frac{\mu_B}{2} g_{1z}$ ,  $\tilde{g}_{z1} - \tilde{g}_{z2} = \frac{\mu_B}{2} g_{2z}$ . This model

Hamiltonian can also be derived from  $\mathbf{k} \cdot \mathbf{p}$  theory and the parameters  $g_{1z}$ ,  $g_{2z}$ ,  $g_{1p}$  and  $g_{2p}$  can be related to the matrix elements of the momentum operator  $\mathbf{p}$  in the  $\mathbf{k} \cdot \mathbf{p}$  theory, with full details given in Appendix C. Now our total Hamiltonian for the bulk states under the z-direction magnetic field is given by  $\hat{H}_B = \hat{H}_{0B} + \hat{H}_Z$ , which can be solved numerically to obtain the Landau level  $E_{N,\eta}^{bulk}(B, k_z)$  with Landau level index  $N$  and band index  $\eta$  under the z-direction magnetic field.

Similar procedure can be applied to the surface effective Hamiltonian (34). With the wave function ansatz  $\Psi_{sur,N} = [g_1^N \varphi_{N-1}, g_2^N \varphi_N]^T$ , the surface Hamiltonian is changed to

$$\begin{aligned} \hat{H}_{sur,B0}(N) &= \tilde{C}_0 + \frac{2NeB_z}{\hbar} \tilde{C}_2 - \frac{\tilde{C}_2 e B_z}{\hbar} \sigma_z \\ &- \sqrt{\frac{2NeB_z}{\hbar}} \tilde{A} \sigma_y, \end{aligned} \quad (46)$$

and the Zeeman type term is given by

$$\hat{H}_{sur,Z} = \frac{\mu_B}{2} g_{sz} \sigma_z B_z + \frac{\mu_B}{2} g_{sp} (\sigma_x B_x + \sigma_y B_y) \quad (47)$$

with  $\frac{\mu_B}{2} g_{sz} = \tilde{g}_{z1} + \tilde{g}_{z2} \alpha_3$  and  $\frac{\mu_B}{2} g_{sp} = \tilde{g}_{xy1} + \tilde{g}_{xy2} \alpha_3$ . The total Hamiltonian for the surface states yields  $\hat{H}_{sur,B} = \hat{H}_{sur,B0} + \hat{H}_{sur,Z}$  and correspondingly the Landau level in z-direction magnetic field  $B_z$  is solved as

$$\begin{aligned} E_s^{sur}(N) &= \tilde{C}_0 + \frac{2NeB_z}{\hbar} \tilde{C}_2 + \\ &s \sqrt{\left( -\frac{\tilde{C}_2 e B_z}{\hbar} + \frac{\mu_B}{2} g_{sz} B_z \right)^2 + \frac{2NeB_z}{\hbar} \tilde{A}^2} \end{aligned} \quad (48)$$

with  $s = \pm$  for  $N = 1, 2, \dots$  and

$$E^{sur}(0) = \tilde{C}_0 + \frac{eB_z}{\hbar} \tilde{C}_2 - \frac{\mu_B}{2} g_{sz} B_z \quad (49)$$

for zero mode  $N = 0$ . Here we note that due to the existence of the quadratic term  $\tilde{C}_2 k_{\parallel}^2$ , the square root dependence of the energy level verse magnetic field is only an approximation applicable for low Landau levels and low magnetic field. For high magnetic field, it will be a combination of the linear contribution and square root contribution. As shown in Fig 6, the energy of the Landau levels are plotted as the function of  $sgn(N)\sqrt{NB_z}$  and the non-linear behavior will appear for high  $\sqrt{NB_z}$ .

In Fig 7 (b), the Landau levels for both bulk states and surface states are plotted as a function of magnetic field. Here we emphasize that for the bulk states, the Landau levels are plotted for the  $k_z = 0$  point (red line in Fig 7 (b)). The dispersion along z direction is also shown in Fig 7 (a) for  $B = 0T$  and (c) for  $B = 20T$ . From Fig 7 (a), we find that the maximum of the valence band is not located at  $k_z = 0$  point for small magnetic field, hence we plot the maximum of valence band as the green lines in Fig 7 (b). When the magnetic field is increased, the bulk gap is also decreased by a significant amount (about 160meV for 5T magnetic field), which is due to the double hump structure for the valence band

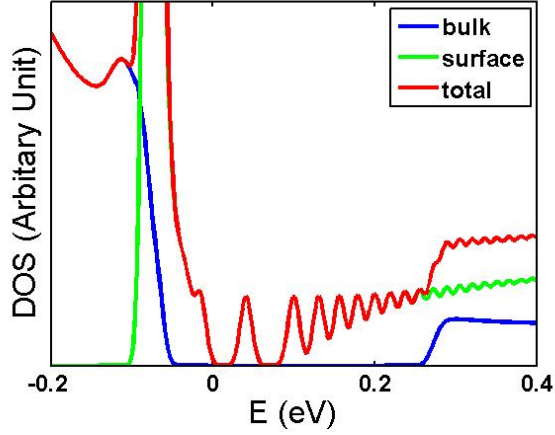


FIG. 8: The density of states (DOS) as a function of energy is plotted with  $B = 10T$  for the bulk (blue line), surface (green line) and total (red line) Landau levels.

dispersion of  $Bi_2Se_3$ . Such decrease may be observed in a magneto-optical measurement.

In order to compare with the scanning tunneling microscope (STM) experiment[22, 23], it is helpful to investigate the local density of states (LDOS) at the surface. The LDOS for the surface states and the bulk states can be obtained by[40]

$$D_{sur}(E, B) = \sum_{N,s} \frac{G}{\sqrt{2\pi}\Gamma} e^{-\frac{(E - E_{N,s}^{sur}(B))^2}{2\Gamma^2}} \quad (50)$$

and

$$D_{bulk}(E, B) = L_0 \int \frac{dk_z}{2\pi} \sum_{N,s} \frac{G}{\sqrt{2\pi}\Gamma} e^{-\frac{(E - E_{N,s}^{bulk}(B, k_z))^2}{2\Gamma^2}} \quad (51)$$

respectively, where  $G = \frac{eB_s}{2\pi\hbar} = \frac{1}{2\pi l_c^2}$  is the degeneracy of each Landau level and  $\Gamma$  is the broadening. In order to compare the bulk LDOS with the surface LDOS, we require to introduce a length scale  $L_0$  which represents the detection depth of STM. Here we simply take  $L_0$  to be the thickness of one quintuple layer. Furthermore the surface states only exist near  $\mathbf{k} = 0$ , thus we need to take a cut-off for the Landau level index  $N$ . With the formula (50) and (51), LDOS for both the bulk and surface Landau levels are shown in Fig. 8. The bulk LDOS shows a gap of about 0.3eV and within the bulk gap, only surface LDOS remains and shows clearly the Landau levels as discreted peaks. The largest Landau gap for surface states is between the 0th and 1th Landau level, about 50meV, which is large enough for the observation of the topological magneto-electric effect[36, 37].

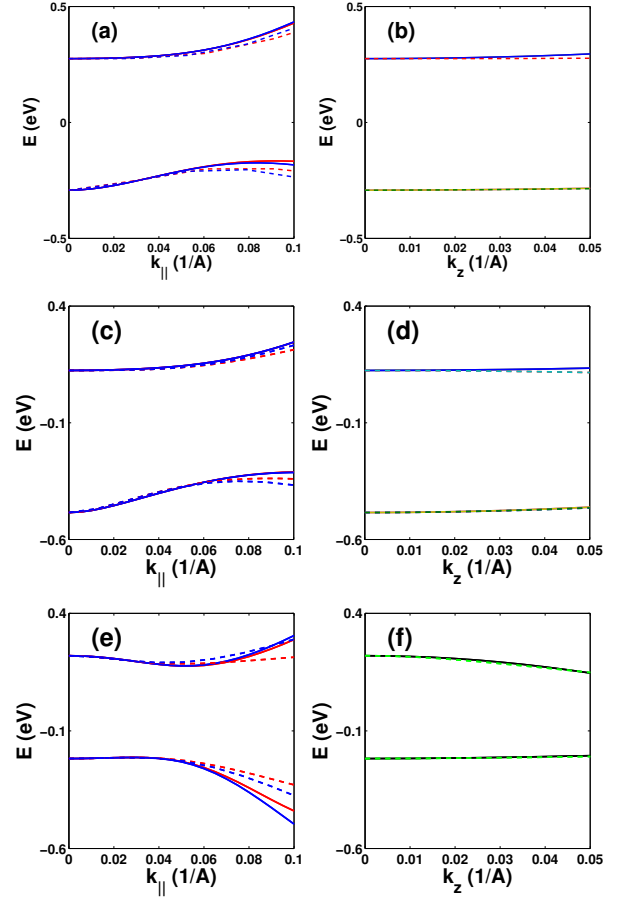


FIG. 9: The energy dispersion obtained from the new model Hamiltonian with eight bands (solid line) is compared with that from *ab initio* calculation (dashed line) for (a), (c) and (e)  $k_x$  and  $k_y$  direction and (b), (d) and (f)  $k_z$  direction. Here (a) and (b) is for  $Bi_2Se_3$ , (c) and (d) is for  $Bi_2Te_3$ , while (e) and (f) is for  $Sb_2Te_3$ . In (a), (c) and (e), the red line represents the dispersion along  $k_x$  direction while the blue line is for  $k_y$  direction.

## VII. NEW MODEL HAMILTONIAN WITH EIGHT BANDS

As we have described above, our model Hamiltonian can capture the salient topological features of the  $Bi_2Se_3$  family of materials. However, for full quantitative fitting with the first principle calculations, we need to expand the basis set. By inspecting carefully the  $\mathbf{k} \cdot \mathbf{p}$  matrix elements, we find that there are strong couplings between the state  $|P1_{\pm}^{\pm}, \pm\frac{1}{2}\rangle$  and the state  $|P2_{\pm}^{-}, \tilde{\Gamma}_{4,5}\rangle$  or  $|P2_{\pm}^{-}, \pm\frac{1}{2}\rangle$ . For example, at the valence band maximum  $k_x \approx 0.07\text{\AA}^{-1}$ , we find that these couplings can be as large as the energy gap between these states. Therefore it is not surprise that our model Hamiltonian with four bands is not suitable in this regime. The strong couplings between these states indicate that if we want to describe this material more accurately, we need to fur-

ther include the states  $|P2^-, \tilde{\Gamma}_{4,5}\rangle$  and  $|P2^-, \pm\frac{1}{2}\rangle$  into our model Hamiltonian. In the basis sequence  $|P1^+, \frac{1}{2}\rangle$ ,  $|P1^+, -\frac{1}{2}\rangle$ ,  $|P2^+, \frac{1}{2}\rangle$ ,  $|P2^+, -\frac{1}{2}\rangle$ ,  $|P1^-, \tilde{\Gamma}_4\rangle$ ,  $|P2^-, \tilde{\Gamma}_5\rangle$ ,

$|P2^-, \frac{1}{2}\rangle$  and  $|P2^-, -\frac{1}{2}\rangle$ , following the similar perturbation procedure, we find that our model Hamiltonian is written as

$$\hat{H} = \frac{\hbar^2}{2m_0} \begin{pmatrix} f_1(\mathbf{k}) & 0 & \frac{2}{\hbar}k_z Q_1 & \frac{2}{\hbar}P_1 k_- & \frac{2}{\hbar}Q_2 k_+ & \frac{2}{\hbar}k_+ P_2 & \frac{2}{\hbar}k_z Q_3 & \frac{2}{\hbar}k_- P_3 \\ & f_1(\mathbf{k}) & \frac{2}{\hbar}k_+ P_1^* & -\frac{2}{\hbar}k_z Q_1^* & -\frac{2}{\hbar}P_2^* k_- & \frac{2}{\hbar}Q_2^* k_- & \frac{2}{\hbar}P_3^* k_+ & -\frac{2}{\hbar}Q_3^* k_z \\ & & f_3(\mathbf{k}) & 0 & g_{35}(\mathbf{k}) & g_{36}(\mathbf{k}) & f_{37}(\mathbf{k}) & -g_{47}^*(-\mathbf{k}) \\ & & & f_3(\mathbf{k}) & g_{36}^*(-\mathbf{k}) & -g_{35}^*(-\mathbf{k}) & g_{47}(\mathbf{k}) & f_{37}^*(-\mathbf{k}) \\ & & & & f_5(\mathbf{k}) & 0 & -g_{68}^*(-\mathbf{k}) & g_{58}(\mathbf{k}) \\ & & & & & f_5(\mathbf{k}) & g_{58}^*(-\mathbf{k}) & g_{68}(\mathbf{k}) \\ & & & & & & f_7(\mathbf{k}) & 0 \\ & & & & & & & f_7(\mathbf{k}) \end{pmatrix} \quad (52)$$

with

$$f_{i(ij)}(\mathbf{k}) = F_{i(ij)}k_z^2 + K_{i(ij)}k_{\parallel}^2 \quad (53)$$

$$g_{ij}(\mathbf{k}) = U_{ij}k_z k_+ + V_{ij}k_-^2. \quad (54)$$

The parameters  $F_{ij}$ ,  $K_{ij}$ ,  $U_{ij}$  and  $V_{ij}$  can now also be determined by the perturbation theory, which is shown in appendix C. In this Hamiltonian, time-reversal symmetry is already satisfied. Furthermore,  $R_2$  rotation symmetry yields that  $U_{35} = U_{36}^*$ ,  $V_{35} = -V_{36}^*$ ,  $U_{58} = -U_{68}^*$  and  $V_{58} = V_{68}^*$ . The obtained parameters are listed in table V and the band dispersion is found to fit well with that of *ab initio* calculation, as shown in Fig 9. This demonstrate that the eight band model is suitable to serve as the basis of the quantitative study of  $Bi_2Se_3$  family of materials.

We would like to make some more remarks about the eight band model. Firstly, in our model Hamiltonian with four bands, the leading term that breaks the in-plane full rotation symmetry down to  $R_3$  symmetry is the third order in perturbation, while in the eight band model, it is the second order coupling  $g_{ij}$ . These type of terms exist because the states  $|P2^-, \tilde{\Gamma}_{4,5}\rangle$  themselves break the rotation symmetry according to the expression (13) and (14). Secondly, it is interesting to compare the present eight band model with the well-known Kane model for usual III-V or II-VI group semiconductors with zinc-blend structure. In fact there is a one-to-one correspondence between the basis of these two models, in which  $|P1^+, \pm\frac{1}{2}\rangle$  corresponds to the electron band ( $\Gamma_6$ ),  $|P2^+, \pm\frac{1}{2}\rangle$  and  $|P2^-, \Gamma_{4,5}\rangle$  correspond to the light hole and heavy hole bands ( $\Gamma_8$ ), respectively, and  $|P2^-, \pm\frac{1}{2}\rangle$  corresponds to the spin-orbit split-off band ( $\Gamma_7$ ). Therefore, from the symmetry point of view, our model here is nothing but an extension of the Kane model to a crystal structure with lower symmetry.

## VIII. CONCLUSIONS

To summarize, based on the symmetry properties and the  $\mathbf{k} \cdot \mathbf{p}$  perturbation theory, we systematically derived a model Hamiltonian for the 3D TI in the  $Bi_2Se_3$  class of materials. Our model Hamiltonian captures the main low energy physics, such as the inverted band structure and topologically protected surface states. The topological surface states have well defined spin texture, which can be traced back to the sign of the atomic SOC in these materials. Furthermore, the Landau levels of a z-direction magnetic field for both bulk states and surface states are calculated. The gap of bulk Landau levels is shown to decrease when magnetic field increases, which may be observed in a magneto-optical spectroscopy. Within the bulk gap, the surface Landau levels appears as discrete peaks for the LDOS, which can be detected by STM. We also analyze the quantitative limitation of our model Hamiltonian with four bands and show that a new model Hamiltonian with eight energy bands can describe  $Bi_2Se_3$  type of materials quantitatively, which will be useful in the future comparison with experiments.

## IX. ACKNOWLEDGMENTS

We would like to thank Yulin Chen, Aahron Kapitulnik, Zhixun Shen and Qikun Xue for the helpful discussion. This work is supported by the Department of Energy, Office of Basic Energy Sciences, Division of Materials Sciences and Engineering, under contract DE-AC02-76SF00515 and by the Keck Foundation. C.X. Liu acknowledge financial support by the Alexander von Humboldt Foundation of Germany. This work is also supported by the NSF of China, the National Basic Research Program of China (No. 2007CB925000), the International Science and Technology Cooperation Program of China (No. 2008DFB00170).

### Appendix A: Symmetry property of group $D_{3d}^5$

As described in the text, the group  $D_{3d}^5$  is generated by a three-fold rotation operator  $R_3$ , a two-fold rotation operator  $R_2$  and an inversion operator  $P$ . It has six classes and correspondingly six irreducible representations,  $\tilde{\Gamma}_1^\pm$ ,  $\tilde{\Gamma}_2^\pm$  and  $\tilde{\Gamma}_3^\pm$  with the upper index  $\pm$  denoting the parity of the representation. Here we use  $\tilde{\Gamma}$  to denote the representation at  $\Gamma$  point in BZ to avoid confusion with the Dirac  $\Gamma$  matrices. The character table of  $D_{3d}^5$  is given in table (I)[39].

TABLE I: The character table for  $D_{3d}^5(R\bar{3}m)$ .

| $D_{3d}(\bar{3}m)$   | $E$ | $2R_3$ | $3R_2$ | $P$ | $2PR_3$ | $3PR_2$ |
|----------------------|-----|--------|--------|-----|---------|---------|
| $\tilde{\Gamma}_1^+$ | 1   | 1      | 1      | 1   | 1       | 1       |
| $\tilde{\Gamma}_2^+$ | 1   | 1      | -1     | 1   | 1       | -1      |
| $\tilde{\Gamma}_3^+$ | 2   | -1     | 0      | 2   | -1      | 0       |
| $\tilde{\Gamma}_1^-$ | 1   | 1      | 1      | -1  | -1      | -1      |
| $\tilde{\Gamma}_2^-$ | 1   | 1      | -1     | -1  | -1      | 1       |
| $\tilde{\Gamma}_3^-$ | 2   | -1     | 0      | -2  | 1       | 0       |

After taking into account the spin, the  $\mathcal{C} = 2\pi$  rotation induces a minus sign for the spin part, so that the elements of the group is doubled, which is the so-called double group. For  $D_{3d}^5$ , the class and irreducible representation of the double group is also doubled. The char-

acter table for the double group of  $D_{3d}^5$  is given in table (II)[39].

When constructing the double group, it is useful to consider the decomposition of the direct product of  $\tilde{\Gamma}_{1,2,3}^\pm$  and spinor representation  $\tilde{\Gamma}_6$ , which is given by

$$\tilde{\Gamma}_3^\pm \otimes \tilde{\Gamma}_6^\pm = \tilde{\Gamma}_4^\pm + \tilde{\Gamma}_5^\pm + \tilde{\Gamma}_6^\pm \quad (\text{A1})$$

$$\tilde{\Gamma}_1^\pm \otimes \tilde{\Gamma}_6^\pm = \tilde{\Gamma}_6^\pm \quad (\text{A2})$$

$$\tilde{\Gamma}_2^\pm \otimes \tilde{\Gamma}_6^\pm = \tilde{\Gamma}_6^\pm. \quad (\text{A3})$$

Furthermore when considering about the matrix elements of  $\mathbf{k} \cdot \mathbf{p}$  theory, the following direct products will be quite helpful.

$$(\tilde{\Gamma}_6^\pm)^* \otimes \tilde{\Gamma}_6^\pm = \tilde{\Gamma}_1^\pm + \tilde{\Gamma}_2^\pm + \tilde{\Gamma}_3^\pm \quad (\text{A4})$$

$$(\tilde{\Gamma}_6^\pm)^* \otimes \tilde{\Gamma}_6^\pm = \tilde{\Gamma}_1^\pm + \tilde{\Gamma}_2^\pm + \tilde{\Gamma}_3^\pm \quad (\text{A5})$$

$$(\tilde{\Gamma}_6^\pm)^* \otimes \tilde{\Gamma}_4^\pm = \tilde{\Gamma}_3^\pm \quad (\text{A6})$$

$$(\tilde{\Gamma}_6^\pm)^* \otimes \tilde{\Gamma}_4^\pm = \tilde{\Gamma}_3^\mp \quad (\text{A7})$$

$$(\tilde{\Gamma}_6^\pm)^* \otimes \tilde{\Gamma}_5^\pm = \tilde{\Gamma}_3^\pm \quad (\text{A8})$$

$$(\tilde{\Gamma}_6^\pm)^* \otimes \tilde{\Gamma}_5^\pm = \tilde{\Gamma}_3^\mp \quad (\text{A9})$$

$$(\tilde{\Gamma}_{4(5)}^+)^* \otimes \tilde{\Gamma}_{4(5)}^- = \tilde{\Gamma}_1^- \quad (\text{A10})$$

$$(\tilde{\Gamma}_{4(5)}^+)^* \otimes \tilde{\Gamma}_{5(4)}^- = \tilde{\Gamma}_2^- \quad (\text{A11})$$

TABLE II: The character table for the double group of  $D_{3d}^5(R\bar{3}m)$ .

| $D_{3d}(\bar{3}m)$   | $E$ | $2R_3$ | $3R_2$ | $P$ | $2PR_3$ | $3PR_2$ | $C$ | $2CR_3$ | $3CR_2$ | $CP$ | $2CPR_3$ | $3CPR_2$ |
|----------------------|-----|--------|--------|-----|---------|---------|-----|---------|---------|------|----------|----------|
| $\tilde{\Gamma}_1^+$ | 1   | 1      | 1      | 1   | 1       | 1       | 1   | 1       | 1       | 1    | 1        | 1        |
| $\tilde{\Gamma}_2^+$ | 1   | 1      | -1     | 1   | 1       | -1      | 1   | 1       | -1      | 1    | 1        | -1       |
| $\tilde{\Gamma}_3^+$ | 2   | -1     | 0      | 2   | -1      | 0       | 2   | -1      | 0       | 2    | -1       | 0        |
| $\tilde{\Gamma}_4^+$ | 1   | -1     | i      | 1   | -1      | i       | -1  | 1       | -i      | -1   | 1        | -i       |
| $\tilde{\Gamma}_5^+$ | 1   | -1     | -i     | 1   | -1      | -i      | -1  | 1       | i       | -1   | 1        | i        |
| $\tilde{\Gamma}_6^+$ | 2   | 1      | 0      | 2   | 1       | 0       | -2  | -1      | 0       | -2   | -1       | 0        |
| $\tilde{\Gamma}_1^-$ | 1   | 1      | 1      | -1  | -1      | -1      | 1   | 1       | 1       | -1   | -1       | -1       |
| $\tilde{\Gamma}_2^-$ | 1   | 1      | -1     | -1  | -1      | 1       | 1   | 1       | -1      | -1   | -1       | 1        |
| $\tilde{\Gamma}_3^-$ | 2   | -1     | 0      | -2  | 1       | 0       | 2   | -1      | 0       | -2   | 1        | 0        |
| $\tilde{\Gamma}_4^-$ | 1   | -1     | i      | -1  | 1       | -i      | -1  | 1       | -i      | 1    | -1       | i        |
| $\tilde{\Gamma}_5^-$ | 1   | -1     | -i     | -1  | 1       | i       | -1  | 1       | i       | 1    | -1       | -i       |
| $\tilde{\Gamma}_6^-$ | 2   | 1      | 0      | -2  | -1      | 0       | -2  | -1      | 0       | 2    | 1        | 0        |

### Appendix B: $\Gamma$ matrix

$$\Gamma_4 = 1 \otimes \tau_2 \quad \Gamma_5 = 1 \otimes \tau_3, \quad (\text{B1})$$

The five Dirac  $\Gamma$  matrices can be defined as

$$\Gamma_1 = \sigma_1 \otimes \tau_1 \quad \Gamma_2 = \sigma_2 \otimes \tau_1 \quad \Gamma_3 = \sigma_3 \otimes \tau_1$$

which satisfies Clifford algebra  $\{\Gamma_a, \Gamma_b\} = 2\delta_{ab}$ . The other ten  $\Gamma$  matrices are given by  $\Gamma_{ab} = [\Gamma_a, \Gamma_b]/2i$ . Explicitly,

$\Gamma_{ab}$  is given by

$$\Gamma_{ij} = [\sigma_i \otimes \tau_1, \sigma_j \otimes \tau_1]/2i = \varepsilon_{ijk} \sigma_k \otimes 1 \quad (\text{B2})$$

$$\Gamma_{i4} = [\sigma_i \otimes \tau_1, 1 \otimes \tau_2]/2i = \sigma_i \otimes \tau_3 \quad (\text{B3})$$

$$\Gamma_{i5} = [\sigma_i \otimes \tau_1, 1 \otimes \tau_3]/2i = -\sigma_i \otimes \tau_2 \quad (\text{B4})$$

$$\Gamma_{45} = [1 \otimes \tau_2, 1 \otimes \tau_3]/2i = 1 \otimes \tau_1 \quad (\text{B5})$$

where  $i, j = 1, 2, 3$ . Now let's check the properties of the fifteen  $\Gamma$  matrices under the time reversal operation  $T$  and inversion operation  $P$ . We assume the  $\Gamma$  matrices are written in the basis  $|P1_+^+, \frac{1}{2}\rangle$ ,  $|P2_-^-, \frac{1}{2}\rangle$ ,  $|P1_-^+, -\frac{1}{2}\rangle$  and  $|P2_+^-, -\frac{1}{2}\rangle$ , then the transformation matrix of the symmetry operation has been obtained in Sec. III. With these transformation matrices, we have

$$T\Gamma_i T^{-1} = P\Gamma_i P^{-1} = -\Gamma_i, \quad i = 1, 2, 3, 4 \quad (\text{B6})$$

$$T\Gamma_5 T^{-1} = P\Gamma_5 P^{-1} = \Gamma_5 \quad (\text{B7})$$

In fact  $P$  operator is exactly  $\Gamma_5$  here.

$$T\Gamma_{ij} T^{-1} = -P\Gamma_{ij} P^{-1} = -\Gamma_{ij}, \quad (\text{B8})$$

$$T\Gamma_{i4} T^{-1} = -P\Gamma_{i4} P^{-1} = -\Gamma_{i4}, \quad (\text{B9})$$

$$T\Gamma_{i5} T^{-1} = -P\Gamma_{i5} P^{-1} = \Gamma_{i5}, \quad (\text{B10})$$

$$T\Gamma_{45} T^{-1} = -P\Gamma_{45} P^{-1} = \Gamma_{45}. \quad (\text{B11})$$

where  $i, j = 1, 2, 3$ .

Next let's consider about  $R_2$ .

$$R_2 \Gamma_{1,4} R_2^{-1} = -\Gamma_{1,4}, \quad (\text{B12})$$

$$R_2 \Gamma_{2,3,5} R_2^{-1} = \Gamma_{2,3,5} \quad (\text{B13})$$

$$R_2 \Gamma_{12,31,24,34,15,45} R_2^{-1} = -\Gamma_{12,31,24,34,15,45}, \quad (\text{B14})$$

$$R_2 \Gamma_{23,14,25,35} R_2^{-1} = \Gamma_{23,14,25,35}. \quad (\text{B15})$$

Finally let's talk about the three fold rotation symmetry. Under the rotation operation  $R_z(\theta)$ , the  $\Gamma$  matrices are transformed as  $\Gamma'(\theta) = e^{i\frac{\Sigma}{2}\theta} \Gamma e^{-i\frac{\Sigma}{2}\theta}$ , then

$$\frac{d\Gamma'(\theta)}{d\theta} = \frac{i}{2} [\Sigma, \Gamma'(\theta)] \quad (\text{B16})$$

Therefore, the transformation properties of  $\Gamma$  matrix under the rotation operation are determined by the commutation relation  $[\Sigma, \Gamma]$ . The commutation relations for  $\Gamma$  matrix are listed as follows:

$$[\Sigma, \Gamma_1] = 2i\Gamma_2, \quad [\Sigma, \Gamma_2] = -2i\Gamma_1 \quad (\text{B17})$$

$$[\Sigma, \Gamma_3] = [\Sigma, \Gamma_4] = [\Sigma, \Gamma_5] = 0,$$

$$[\Sigma, \Gamma_{12}] = 0, \quad [\Sigma, \Gamma_{34}] = 0 \quad (\text{B18})$$

$$[\Sigma, \Gamma_{31}] = -2i\Gamma_{23} \quad [\Sigma, \Gamma_{23}] = 2i\Gamma_{31} \quad (\text{B19})$$

$$[\Sigma, \Gamma_{14}] = 2i\Gamma_{24} \quad [\Sigma, \Gamma_{24}] = -2i\Gamma_{14} \quad (\text{B20})$$

$$[\Sigma, \Gamma_{15}] = 2i\Gamma_{25}, \quad [\Sigma, \Gamma_{25}] = -2i\Gamma_{15} \quad (\text{B21})$$

$$[\Sigma, \Gamma_{35}] = 0, \quad [\Sigma, \Gamma_{45}] = 0 \quad (\text{B22})$$

With the above commutation relations, we can easily solve the equation (B16) and find that

$$\Gamma'_1(\theta) = \Gamma_1 \cos \theta - \Gamma_2 \sin \theta,$$

$$\Gamma'_2(\theta) = \Gamma_1 \sin \theta + \Gamma_2 \cos \theta \quad (\text{B23})$$

$$\Gamma'_3(\theta) = \Gamma_3, \quad \Gamma'_4(\theta) = \Gamma_4 \quad (\text{B24})$$

$$\Gamma'_{23}(\theta) = \Gamma_{23} \cos \theta - \Gamma_{31} \sin \theta,$$

$$\Gamma'_{31}(\theta) = \Gamma_{31} \cos \theta + \Gamma_{23} \sin \theta \quad (\text{B25})$$

$$\Gamma'_{14}(\theta) = \Gamma_{14} \cos \theta - \Gamma_{24} \sin \theta,$$

$$\Gamma'_{24}(\theta) = \Gamma_{14} \sin \theta + \Gamma_{24} \cos \theta \quad (\text{B26})$$

$$\Gamma'_{15}(\theta) = \Gamma_{15} \cos \theta - \Gamma_{25} \sin \theta,$$

$$\Gamma'_{25}(\theta) = \Gamma_{15} \sin \theta + \Gamma_{25} \cos \theta \quad (\text{B27})$$

$$\Gamma'_5(\theta) = \Gamma_5, \quad \Gamma'_{34} = \Gamma_{34}, \quad \Gamma'_{12} = \Gamma_{12},$$

$$\Gamma'_{35} = \Gamma_{35}, \quad \Gamma'_{45} = \Gamma_{45} \quad (\text{B28})$$

The above results indicate that under the rotation  $R_3$   $\Gamma_{3,4,5}$  and  $\Gamma_{12,34,35,45}$  behave as scalars (or pseudo-scalars), while the three pairs of operators  $\{\Gamma_{23}, \Gamma_{31}\}$ ,  $\{\Gamma_{14}, \Gamma_{24}\}$  and  $\{\Gamma_{15}, \Gamma_{25}\}$  behave as vectors. The corresponding representation for each  $\Gamma$  matrix is given in table (III).

TABLE III: The character table of  $\Gamma$  matrix and the polynomials of the momentum  $\mathbf{k}$ .

|  | Representation       | $\Gamma$ |
|--|----------------------|----------|
| $\{\Gamma_1, \Gamma_2\}$                   | $\tilde{\Gamma}_3^-$ | -        |
| $\Gamma_3$                                 | $\tilde{\Gamma}_1^-$ | -        |
| $\Gamma_4$                                 | $\tilde{\Gamma}_2^-$ | -        |
| $\Gamma_5$                                 | $\tilde{\Gamma}_1^+$ | +        |
| $\Gamma_{12}$                              | $\tilde{\Gamma}_2^+$ | -        |
| $\{\Gamma_{23}, \Gamma_{31}\}$             | $\tilde{\Gamma}_3^+$ | -        |
| $\{\Gamma_{14}, \Gamma_{24}\}$             | $\tilde{\Gamma}_3^+$ | -        |
| $\{\Gamma_{15}, \Gamma_{25}\}$             | $\tilde{\Gamma}_3^-$ | +        |
| $\Gamma_{34}$                              | $\tilde{\Gamma}_2^+$ | -        |
| $\Gamma_{35}$                              | $\tilde{\Gamma}_1^+$ | +        |
| $\Gamma_{45}$                              | $\tilde{\Gamma}_2^-$ | +        |
| $\{k_x, k_y\}$                             | $\tilde{\Gamma}_3^-$ | -        |
| $k_z, k_z^3$                               | $\tilde{\Gamma}_2^-$ | -        |
| $1, k_x^2 + k_y^2, k_z^2$                  | $\tilde{\Gamma}_1^+$ | +        |
| $\{k_x^2 - k_y^2, 2k_x k_y\}$              | $\tilde{\Gamma}_3^+$ | +        |
| $k_x^3 - 3k_x k_y^2$                       | $\tilde{\Gamma}_1^-$ | -        |
| $3k_x^2 k_y - k_y^3$                       | $\tilde{\Gamma}_2^-$ | -        |
| $\{k_x^3 + k_x k_y^2, k_x^2 k_y + k_y^3\}$ | $\tilde{\Gamma}_3^-$ | -        |
| $\{B_x, B_y\}$                             | $\tilde{\Gamma}_3^+$ | -        |
| $B_z$                                      | $\tilde{\Gamma}_2^+$ | -        |

### Appendix C: Parameters in $\mathbf{k} \cdot \mathbf{p}$ theory

In this appendix, we hope to show the detail results from  $\mathbf{k} \cdot \mathbf{p}$  theory. First let's consider the constraint for the matrix elements of the momentum from the  $D_{3d}^5$  symmetry. As described above, the eigen-states can be denoted by  $|\Lambda^\pm, \alpha\rangle$  with  $\Lambda = P1_\pm, P2_\pm$  and  $\alpha = \pm\frac{1}{2}, \pm\frac{3}{2}$ . The states  $|\Lambda, \pm 1/2\rangle$  belong to  $\tilde{\Gamma}_6^\pm$  representation. For

$|\Lambda, \pm 3/2\rangle$ , as described above, we need to re-combine these two states as

$$|\Lambda^\pm, \tilde{\Gamma}_4\rangle = \frac{1}{\sqrt{2}}(|\Lambda^\pm, 3/2\rangle + |\Lambda^\pm, -3/2\rangle) \quad (\text{C1})$$

$$|\Lambda^\pm, \tilde{\Gamma}_5\rangle = \frac{1}{\sqrt{2}}(|\Lambda^\pm, 3/2\rangle - |\Lambda^\pm, -3/2\rangle), \quad (\text{C2})$$

which belong to  $\tilde{\Gamma}_4$  and  $\tilde{\Gamma}_5$  representation respectively. The expressions (A4) ~ (A11) give the decomposition of the direct product of these states. The momentum  $p_x, p_y$  belongs to  $\tilde{\Gamma}_3^-$  representation, while  $p_z$  belongs to  $\tilde{\Gamma}_2^-$  representation, therefore we require that the decomposition of the direct product of the eigen-states also include  $\tilde{\Gamma}_3^-$  and  $\tilde{\Gamma}_2^-$  to obtain non-zero matrix elements. For example, the direct product of  $\tilde{\Gamma}_6^\pm$  and  $\tilde{\Gamma}_{4,5}^\pm$  doesn't contain  $\tilde{\Gamma}_2$ , which indicates that the matrix element  $\langle \Lambda_1, \pm 1/2 | p_z | \Lambda_2, \tilde{\Gamma}_{4,5} \rangle$  is always zero.

The symmetry operation can further help us to obtain the relation between different matrix elements of the momentum. For example, due to the  $R_3$  rotation symmetry, we have

$$\begin{aligned} & \langle \Lambda_1^+, \frac{1}{2} | p_x | \Lambda_2^-, -\frac{1}{2} \rangle \\ &= \langle \Lambda_1^+, \frac{1}{2} | R_3^\dagger R_3 p_x R_3^\dagger R_3 | \Lambda_2^-, -\frac{1}{2} \rangle \\ &= e^{-i\frac{2\pi}{3}} \langle \Lambda_1^+, \frac{1}{2} | \left( p_x \cos \frac{2\pi}{3} - p_y \sin \frac{2\pi}{3} \right) | \Lambda_2^-, -\frac{1}{2} \rangle \\ &\rightarrow \langle \Lambda_1^+, \frac{1}{2} | p_x | \Lambda_2^-, -\frac{1}{2} \rangle = i \langle \Lambda_1^+, \frac{1}{2} | p_y | \Lambda_2^-, -\frac{1}{2} \rangle. \quad (\text{C3}) \end{aligned}$$

Finally we can define the independent component of the matrix elements as follows.

$$\begin{aligned} & \langle \Lambda_1^+, \frac{1}{2} | p_x | \Lambda_2^-, -\frac{1}{2} \rangle = \langle \Lambda_1^+, -\frac{1}{2} | p_x | \Lambda_2^-, \frac{1}{2} \rangle \\ &= i \langle \Lambda_1^+, \frac{1}{2} | p_y | \Lambda_2^-, -\frac{1}{2} \rangle = -i \langle \Lambda_1^+, -\frac{1}{2} | p_y | \Lambda_2^-, \frac{1}{2} \rangle \\ &= P_{\Lambda_1^+, \Lambda_2^-} \quad (\text{C4}) \end{aligned}$$

$$\begin{aligned} & \langle \Lambda_1^+, \frac{1}{2} | p_z | \Lambda_2^-, \frac{1}{2} \rangle = -\langle \Lambda_1^+, -\frac{1}{2} | p_z | \Lambda_2^-, -\frac{1}{2} \rangle \\ &= Q_{\Lambda_1^+, \Lambda_2^-} \quad (\text{C5}) \end{aligned}$$

$$\begin{aligned} & \langle \Lambda_1^\pm, \frac{1}{2} | p_x | \Lambda_2^\mp, \tilde{\Gamma}_4 \rangle = -i \langle \Lambda_1^\pm, -\frac{1}{2} | p_x | \Lambda_2^\mp, \tilde{\Gamma}_4 \rangle \\ &= -i \langle \Lambda_1^\pm, \frac{1}{2} | p_y | \Lambda_2^\mp, \tilde{\Gamma}_4 \rangle = \langle \Lambda_1^\pm, -\frac{1}{2} | p_y | \Lambda_2^\mp, \tilde{\Gamma}_4 \rangle \\ &= M_{\Lambda_1^\pm, \Lambda_2^\mp} \quad (\text{C6}) \end{aligned}$$

$$\begin{aligned} & \langle \Lambda_1^\pm, \frac{1}{2} | p_x | \Lambda_2^\mp, \tilde{\Gamma}_5 \rangle = i \langle \Lambda_1^\pm, -\frac{1}{2} | p_x | \Lambda_2^\mp, \tilde{\Gamma}_5 \rangle \\ &= -i \langle \Lambda_1^\pm, \frac{1}{2} | p_y | \Lambda_2^\mp, \tilde{\Gamma}_5 \rangle = -\langle \Lambda_1^\pm, -\frac{1}{2} | p_y | \Lambda_2^\mp, \tilde{\Gamma}_5 \rangle \\ &= N_{\Lambda_1^\pm, \Lambda_2^\mp} \quad (\text{C7}) \end{aligned}$$

$$\langle \Lambda_1^+, \tilde{\Gamma}_4 | p_z | \Lambda^-, \tilde{\Gamma}_4 \rangle = R_{\Lambda_1^+, \Lambda_2^-} \quad (\text{C8})$$

$$\langle \Lambda_1^+, \tilde{\Gamma}_5 | p_z | \Lambda^-, \tilde{\Gamma}_5 \rangle = S_{\Lambda_1^+, \Lambda_2^-} \quad (\text{C9})$$

Here it is more convenient of use  $p_\pm = p_x \pm ip_y$ , which leads to

$$\begin{aligned} & \langle \Lambda_1^+, \frac{1}{2} | p_+ | \Lambda_2^-, -\frac{1}{2} \rangle = \langle \Lambda_1^+, -\frac{1}{2} | p_- | \Lambda_2^-, \frac{1}{2} \rangle \\ &= 2P_{\Lambda_1^+, \Lambda_2^-} \quad (\text{C10}) \end{aligned}$$

$$\begin{aligned} & \langle \Lambda_1^+, \frac{1}{2} | p_- | \Lambda_2^-, -\frac{1}{2} \rangle = \langle \Lambda_1^+, -\frac{1}{2} | p_+ | \Lambda_2^-, \frac{1}{2} \rangle \\ &= 0 \quad (\text{C11}) \end{aligned}$$

$$\begin{aligned} & \langle \Lambda_1^\pm, \frac{1}{2} | p_- | \Lambda_2^\mp, \Gamma_4 \rangle = -i \langle \Lambda_1^\pm, -\frac{1}{2} | p_+ | \Lambda_2^\mp, \Gamma_4 \rangle \\ &= 2M_{\Lambda_1^\pm, \Lambda_2^\mp} \quad (\text{C12}) \end{aligned}$$

$$\begin{aligned} & \langle \Lambda_1^\pm, \frac{1}{2} | p_+ | \Lambda_2^\mp, \Gamma_4 \rangle = -i \langle \Lambda_1^\pm, -\frac{1}{2} | p_- | \Lambda_2^\mp, \Gamma_4 \rangle \\ &= 0 \quad (\text{C13}) \end{aligned}$$

$$\begin{aligned} & \langle \Lambda_1^\pm, \frac{1}{2} | p_- | \Lambda_2^\mp, \Gamma_5 \rangle = i \langle \Lambda_1^\pm, -\frac{1}{2} | p_+ | \Lambda_2^\mp, \Gamma_5 \rangle \\ &= 2N_{\Lambda_1^\pm, \Lambda_2^\mp} \quad (\text{C14}) \end{aligned}$$

$$\begin{aligned} & \langle \Lambda_1^\pm, \frac{1}{2} | p_+ | \Lambda_2^\mp, \Gamma_5 \rangle = i \langle \Lambda_1^\pm, -\frac{1}{2} | p_- | \Lambda_2^\mp, \Gamma_5 \rangle \\ &= 0 \quad (\text{C15}) \end{aligned}$$

Time reversal symmetry indicates that  $P_{\Lambda_1^+, \Lambda_2^-}$ ,  $Q_{\Lambda_1^+, \Lambda_2^-}$  can be chosen to be real ( $P_{\Lambda_1^+, \Lambda_2^-} = P_{\Lambda_1^+, \Lambda_2^-}^*$ ,  $Q_{\Lambda_1^+, \Lambda_2^-} = Q_{\Lambda_1^+, \Lambda_2^-}^*$ ) while  $M_{\Lambda_1^\pm, \Lambda_2^\mp} = iN_{\Lambda_1^\pm, \Lambda_2^\mp}^*$  and  $R_{\Lambda_1^+, \Lambda_2^-} = -S_{\Lambda_1^+, \Lambda_2^-}^*$ . Since the matrix element between  $|P1_\pm^\pm, \pm\frac{1}{2}\rangle$  and  $|P2_\pm^\pm, \pm\frac{1}{2}\rangle$  is quite important, we denote

$$\begin{aligned} & \langle P1_-^+, \frac{1}{2} | p_x | P2_+^-, -\frac{1}{2} \rangle = \langle P1_-^+, -\frac{1}{2} | p_x | P2_+^-, \frac{1}{2} \rangle = \\ & i \langle P1_-^+, \frac{1}{2} | p_y | P2_+^-, -\frac{1}{2} \rangle = -i \langle P1_-^+, -\frac{1}{2} | p_x | P2_+^-, \frac{1}{2} \rangle \\ &= P_0 \quad (\text{C16}) \end{aligned}$$

$$\begin{aligned} & \langle P1_-^+, \frac{1}{2} | p_z | P2_+^-, \frac{1}{2} \rangle = -\langle P1_-^+, -\frac{1}{2} | p_z | P2_+^-, -\frac{1}{2} \rangle \\ &= Q_0 \quad (\text{C17}) \end{aligned}$$

Now we consider the perturbation theory. The degenerate perturbation formulism is given by

$$H_{mm'}^{(0)} = E_m \delta_{mm'} \quad (\text{C18})$$

$$H_{mm'}^{(1)} = H'_{mm'} \quad (\text{C19})$$

$$\begin{aligned} & H_{mm'}^{(2)} = \frac{1}{2} \sum_l H'_{ml} H'_{lm'} \left( \frac{1}{E_m - E_l} \right. \\ & \left. + \frac{1}{E_{m'} - E_l} \right) \quad (\text{C20}) \end{aligned}$$

$$\begin{aligned} & H_{mm'}^{(3)} = -\frac{1}{2} \sum_{l, m''} \left[ \frac{H'_{ml} H'_{lm''} H'_{m''m'}}{(E_m - E_l)(E_{m''} - E_l)} \right. \\ & \left. + \frac{H'_{mm''} H'_{m''l} H'_{lm'}}{(E_m - E_l)(E_{m''} - E_l)} \right] \\ & + \frac{1}{2} \sum_{l, l'} H'_{ml} H'_{l'l'} H'_{l'm'} \left[ \frac{1}{(E_m - E_l)(E_m - E_{l'})} \right] \end{aligned}$$

$$+ \frac{1}{(E_{m'} - E_l)(E_{m'} - E_{l'})} \Big]. \quad (\text{C21})$$

Here  $m$  and  $m'$  are taken from  $|P1^+, 1/2\rangle = |1\rangle$ ,  $|P2^-, 1/2\rangle = |2\rangle$ ,  $|P1^+, -1/2\rangle = |3\rangle$  and  $|P2^-, -1/2\rangle = |4\rangle$  with the energy  $E_1 = E_3$  and  $E_2 = E_4$  and  $E_1 < E_2$ .  $l$  is taken from the other bands except for these four bands. The expression from perturbation calculation of our model Hamiltonian with four bands is given as follows and the values of the parameters are listed in table IV. For our new model Hamiltonian with eight band model, the perturbation procedure is the same to our model Hamiltonian with four bands and here we only list the values of the parameters in table V.

$$C_0 + M_0 = E_1 \quad (\text{C22})$$

$$C_0 - M_0 = E_2 \quad (\text{C23})$$

$$C_1 + M_1 = \frac{\hbar^2}{2m_0} + \frac{\hbar^2}{m_0^2} \sum_{\Lambda^-} \frac{|Q_{P1^+, \Lambda^-}|^2}{E_1 - E_{\Lambda^-, 1/2}} \quad (\text{C24})$$

$$C_2 + M_2 = \frac{\hbar^2}{2m_0} + \frac{\hbar^2}{m_0^2} \sum_{\Lambda^-} \left( \frac{|P_{P1^+, \Lambda^-}|^2}{E_1 - E_{\Lambda^-, -1/2}} + \frac{|M_{P1^+, \Lambda^-}|^2}{E_1 - E_{\Lambda^-, \Gamma_4}} + \frac{|N_{P1^+, \Lambda^-}|^2}{E_1 - E_{\Lambda^-, \Gamma_5}} \right) \quad (\text{C25})$$

$$C_1 - M_1 = \frac{\hbar^2}{2m_0} + \frac{\hbar^2}{m_0^2} \sum_{\Lambda^-} \frac{|Q_{\Lambda^+, P2^-}|^2}{E_1 - E_{\Lambda^+, 1/2}} \quad (\text{C26})$$

$$C_2 - M_2 = \frac{\hbar^2 k^2}{2m_0} + \frac{\hbar^2}{m_0^2} \sum_{\Lambda^-} \left( \frac{|P_{\Lambda^+, P2^-}|^2}{E_1 - E_{\Lambda^+, -1/2}} + \frac{|M_{\Lambda^+, P2^-}|^2}{E_1 - E_{\Lambda^+, \Gamma_4}} + \frac{|N_{\Lambda^+, P2^-}|^2}{E_1 - E_{\Lambda^+, \Gamma_5}} \right) \quad (\text{C27})$$

$$A_0 = \frac{\hbar}{m_0} P_0 \quad (\text{C28})$$

$$B_0 = \frac{\hbar}{m_0} Q_0 \quad (\text{C29})$$

For  $R_1$  and  $R_2$  term we have

$$R_1 - R_2 = \frac{\hbar^3}{m_0^3} \left[ \sum_{\Lambda} \frac{|M_{P1^+, \Lambda^-}|^2 P_{P1^+, P2^-}}{(E_{P2^-} - E_{\Lambda^-})(E_{P1^+} - E_{\Lambda^-})} - \sum_{\Lambda_1^-, \Lambda_2^+} M_{P1^+, \Lambda_1^-} M_{\Lambda_2^+, \Lambda_1^-}^* P_{\Lambda_2^+, P2^-} \left( \frac{1}{(E_{P1^+} - E_{\Lambda_1^-})(E_{P1^+} - E_{\Lambda_2^+})} + \frac{1}{(E_{P2^-} - E_{\Lambda_1^-})(E_{P2^-} - E_{\Lambda_2^+})} \right) \right] \quad (\text{C30})$$

$$R_1 + R_2 = \frac{\hbar^3}{m_0^3} \left[ - \sum_{\Lambda} \frac{P_{P1^+, P2^-} |M_{P2^-, \Lambda^-}|^2}{(E_{P2^-} - E_{\Lambda^+})(E_{P1^+} - E_{\Lambda^+})} - \sum_{\Lambda_1^-, \Lambda_2^+} P_{P1^+, \Lambda_1^-} M_{\Lambda_1^-, \Lambda_2^+} M_{P2^-, \Lambda_2^+}^* \left( \frac{1}{(E_{P1^+} - E_{\Lambda_1^-})(E_{P1^+} - E_{\Lambda_2^+})} + \frac{1}{(E_{P2^-} - E_{\Lambda_1^-})(E_{P2^-} - E_{\Lambda_2^+})} \right) \right] \quad (\text{C31})$$

Now we study the effect of magnetic field. Under magnetic field, there are two different kinds of contribution. One is the orbital term, which induce the Landau level and has been considered in Sec. VI. The other one is the Zeeman type term, which is described by an effective g factor. In the following we will discuss about the effective g factor in detail. There are two kinds of contributions to the effective g factor. One comes from the atomic g factor, which can be estimated from the *ab initio* calculation. In an atom, the electron spin and orbital angular momentum couples to magnetic field by  $\hat{H}_{Zee} = \frac{\mu_B}{\hbar} (g_l \mathbf{L} + g_s \mathbf{S}) \cdot \mathbf{B} = \frac{\mu_B}{\hbar} g_0 \mathbf{J} \cdot \mathbf{B}$ , where  $\mathbf{J} = \mathbf{S} + \mathbf{L}$  is the total angular momentum and  $g_0$  is so called Lande g-factor. The wave functions for the basis of our model Hamiltonian have been calculated from *ab initio* calculation, which can be projected into the atomic orbitals. Since for each atomic orbitals, the g factor is simply given by  $g_0 = 1 + \frac{J(J+1) - L(L+1) + S(S+1)}{2J(J+1)}$ , the effective  $g_0$  can

be easily calculated, which is found to be  $g_0 \approx 1.2$ . Another contribution to the effective g factor origins from the second order perturbation, which is related to the correction to the effective mass term. The relation between the effective mass and effective g factor in the ordinary semiconductors is known as the Roth's formula[48]. Here the second order correction to g factor is given by

$$g_{1z}^{(2)} = \frac{4}{m_0} \sum_{\Lambda^-, \alpha} \left( \frac{|P_{P1^+, \Lambda^-}|^2}{E_1 - E_{\Lambda^-, -1/2}} - \frac{|M_{P1^+, \Lambda^-}|^2}{E_1 - E_{\Lambda^-, \Gamma_4}} - \frac{|N_{P1^+, \Lambda^-}|^2}{E_1 - E_{\Lambda^-, \Gamma_5}} \right) \quad (\text{C32})$$

$$g_{1p}^{(2)} = \frac{4}{m_0} \sum_{\Lambda^-} \frac{Q_{P1^+, \Lambda^-} P_{P1^+, \Lambda^-}^*}{E_{P1^+} - E_{\Lambda^-, 1/2}} \quad (\text{C33})$$

$$g_{2z}^{(2)} = \frac{4}{m_0} \sum_{\Lambda^+, \alpha} \left( \frac{|P_{\Lambda^+, P2^-}|^2}{E_2 - E_{\Lambda^+, -1/2}} \right)$$

TABLE IV: The summary of the parameters in our model Hamiltonian with four bands.

|                                   | <i>Bi</i> <sub>2</sub> <i>Se</i> <sub>3</sub> | <i>Bi</i> <sub>2</sub> <i>Te</i> <sub>3</sub> | <i>Sb</i> <sub>2</sub> <i>Te</i> <sub>3</sub> |
|-----------------------------------|---|---|---|
| $A_0(\text{eV}\cdot\text{\AA})$   | 3.33  | 2.87  | 3.40  |
| $B_0(\text{eV}\cdot\text{\AA})$   | 2.26  | 0.30  | 0.84  |
| $C_0(\text{eV})$                  | -0.0083                                       | -0.18   | 0.001   |
| $C_1(\text{eV}\cdot\text{\AA}^2)$ | 5.74  | 6.55  | -12.39  |
| $C_2(\text{eV}\cdot\text{\AA}^2)$ | 30.4  | 49.68   | -10.78  |
| $M_0(\text{eV})$                  | -0.28   | -0.30   | -0.22   |
| $M_1(\text{eV}\cdot\text{\AA}^2)$ | 6.86  | 2.79  | 19.64   |
| $M_2(\text{eV}\cdot\text{\AA}^2)$ | 44.5  | 57.38   | 48.51   |
| $R_1(\text{eV}\text{\AA}^3)$      | 50.6  | 45.02   | 103.20  |
| $R_2(\text{eV}\text{\AA}^3)$      | -113.3  | -89.37  | -244.67                                       |
| $g_{1z}$                          | -25.4   | -50.34  | -14.45  |
| $g_{1p}$                          | -4.12   | -2.67   | -2.43   |
| $g_{2z}$                          | 4.10  | 6.88  | 14.32   |
| $g_{2p}$                          | 4.80  | 3.43  | 16.55   |

$$\left. -\frac{|M_{\Lambda^+,P2^-}|^2}{E_2 - E_{\Lambda^+, \Gamma_4}} - \frac{|N_{\Lambda^+,P2^-}|^2}{E_2 - E_{\Lambda^+, \Gamma_5}} \right) \quad (\text{C34})$$

$$g_{2p}^{(2)} = \frac{4}{m_0} \sum_{\Lambda^+} \frac{Q_{\Lambda^+,P2^-}^* P_{\Lambda^+,P2^-}}{E_{P2^-} - E_{\Lambda^+}}. \quad (\text{C35})$$

where  $g_{1z(p)}$  and  $g_{2z(p)}$  are defined in (45). Therefore finally our effective g factor is the summation of the above two different contributions,

$$g_\alpha = g_0 + g_\alpha^{(2)}, \quad \alpha = 1z, 2z, 1p, 2p \quad (\text{C36})$$

and the values of effective g factor are given in table IV. From table (IV), we find that for  $|P1_\pm^\pm, \pm\frac{1}{2}\rangle$  band, there is a strong anisotropy which comes from the large contribution of the second order perturbation of the states  $|P2^-, \pm\frac{3}{2}\rangle$  and  $|P2_\pm^-, \pm\frac{1}{2}\rangle$ .

TABLE V: The summary of the parameters in the eight band effective model.

|  | <i>Bi</i> <sub>2</sub> <i>Se</i> <sub>3</sub> | <i>Bi</i> <sub>2</sub> <i>Te</i> <sub>3</sub> | <i>Sb</i> <sub>2</sub> <i>Te</i> <sub>3</sub> |
|--|---|---|---|
| $P_1(\text{eV}\cdot\text{\AA})$                  | 3.33  | 2.87  | 3.40  |
| $Q_1(\text{eV}\cdot\text{\AA})$                  | 2.26  | 0.30  | 0.84  |
| $P_2(\text{eV}\cdot\text{\AA})$                  | 2.84  | 2.68  | 3.19  |
| $Q_2(\text{eV}\cdot\text{\AA})$                  | 2.84  | 2.68  | 3.19  |
| $P_3(\text{eV}\cdot\text{\AA})$                  | -2.62   | -1.94   | -2.46   |
| $Q_3(\text{eV}\cdot\text{\AA})$                  | 2.48  | 1.23  | 2.11  |
| $F_1(\text{eV}\cdot\text{\AA}^2)$                | 3.73  | 7.16  | 3.82  |
| $K_1(\text{eV}\cdot\text{\AA}^2)$                | 6.52  | 3.72  | 2.49  |
| $F_3(\text{eV}\cdot\text{\AA}^2)$                | -1.12   | 3.76  | -32.03  |
| $K_3(\text{eV}\cdot\text{\AA}^2)$                | -14.0   | -7.70   | -59.28  |
| $F_5(\text{eV}\cdot\text{\AA}^2)$                | 1.50  | -0.62   | -2.26   |
| $K_5(\text{eV}\cdot\text{\AA}^2)$                | -3.11   | -7.17   | -13.00  |
| $F_7(\text{eV}\cdot\text{\AA}^2)$                | 2.71  | 3.77  | 5.04  |
| $K_7(\text{eV}\cdot\text{\AA}^2)$                | -5.08   | 22.27   | 2.40  |
| $U_{35} = U_{36}^*(\text{eV}\cdot\text{\AA}^2)$  | -2.31-7.45i                                   | -2.21-9.85i                                   | -11.31-46.00i                                 |
| $V_{35} = -V_{36}^*(\text{eV}\cdot\text{\AA}^2)$ | -1.05-5.98i                                   | -2.43-3.53i                                   | -4.50-22.80i                                  |
| $F_{37}(\text{eV}\cdot\text{\AA}^2)$             | 2.47  | 4.39  | 16.96   |
| $K_{37}(\text{eV}\cdot\text{\AA}^2)$             | -8.52   | -6.50   | -24.17  |
| $U_{47}(\text{eV}\cdot\text{\AA}^2)$             | -7.86   | -4.29   | -45.46  |
| $V_{47}(\text{eV}\cdot\text{\AA}^2)$             | -8.95i  | -0.83i  | -17.64i                                       |
| $U_{58} = -U_{68}^*(\text{eV}\cdot\text{\AA}^2)$ | -2.31-2.57i                                   | -0.24-3.69i                                   | -2.01-3.98i                                   |
| $V_{58} = V_{68}^*(\text{eV}\cdot\text{\AA}^2)$  | -0.64-4.29i                                   | -0.85-6.64i                                   | 1.28-9.02i                                    |
| $E_1(\text{eV})$                                 | -0.29   | -0.48   | -0.22   |
| $E_3(\text{eV})$                                 | 0.28  | 0.12  | 0.22  |
| $E_5(\text{eV})$                                 | -0.57   | -0.63   | -0.88   |
| $E_7(\text{eV})$                                 | -0.98   | -1.18   | -1.51   |

- 
- [1] H. Zhang, C. Liu, X. Qi, X. Dai, Z. Fang, and S. Zhang, *Nat Phys* **5**, 438 (2009).
- [2] X. Qi and S. Zhang, *Physics Today* **63**, 33 (2010).
- [3] J. E. Moore, *Nature* **464**, 194 (2010).
- [4] M. Z. Hasan and C. L. Kane, arxiv: cond-mat/1002.3895 (2010).
- [5] B. A. Bernevig, T. L. Hughes, and S.C. Zhang, *Science* **314**, 1757 (2006).
- [6] M. König, S. Wiedmann, C. Brüne, A. Roth, H. Buhmann, L. Molenkamp, X.-L. Qi, and S.-C. Zhang, *Science* **318**, 766 (2007).
- [7] A. Roth, C. Brune, H. Buhmann, L. W. Molenkamp, J. Maciejko, X. Qi, and S. Zhang, *Science* **325**, 294 (2009).
- [8] L. Fu and C. L. Kane, *Phys. Rev. B* **76**, 045302 (2007).
- [9] D. Hsieh, D. Qian, L. Wray, Y. Xia, Y. S. Hor, R. J. Cava, and M. Z. Hasan, *Nature* **452**, 970 (2008).
- [10] Y. Xia, D. Qian, D. Hsieh, L. Wray, A. Pal, H. Lin, A. Bansil, D. Grauer, Y. S. Hor, R. J. Cava, et al., *Nat Phys* **5**, 398 (2009).
- [11] Y. L. Chen, J. G. Analytis, J. Chu, Z. K. Liu, S. Mo, X. L. Qi, H. J. Zhang, D. H. Lu, X. Dai, Z. Fang, et al., *Science* **325**, 178 (2009).
- [12] D. Hsieh, Y. Xia, D. Qian, L. Wray, F. Meier, J. H. Dil, J. Osterwalder, L. Patthey, A. V. Fedorov, H. Lin, et al., *Phys. Rev. Lett.* **103**, 146401 (2009).
- [13] Y. S. Hor, A. J. Williams, J. G. Checkelsky, P. Roushan, J. Seo, Q. Xu, H. W. Zandbergen, A. Yazdani, N. P. Ong, and R. J. Cava, *Phys. Rev. Lett.* **104**, 057001 (2010).
- [14] Z. Alpichshev, J. G. Analytis, J. Chu, I. R. Fisher, Y. L. Chen, Z. X. Shen, A. Fang, and A. Kapitulnik, *Phys. Rev. Lett.* **104**, 016401 (2010).
- [15] D. Kong, J. C. Randel, H. Peng, J. J. Cha, S. Meister, K. Lai, Y. Chen, Z. Shen, H. C. Manoharan, and Y. Cui, *Nano Letters* **10**, 329 (2010).
- [16] J. J. Cha, J. R. Williams, D. Kong, S. Meister, H. Peng, A. J. Bestwick, P. Gallagher, D. Goldhaber-Gordon, and Y. Cui, *Nano Letters* **10**, 1076 (2010).
- [17] H. Peng, K. Lai, D. Kong, S. Meister, Y. Chen, X. Qi, S. Zhang, Z. Shen, and Y. Cui, *Nat Mater* **9**, 225 (2010).
- [18] D. Hsieh, Y. Xia, D. Qian, L. Wray, J. H. Dil, F. Meier, J. Osterwalder, L. Patthey, J. G. Checkelsky, N. P. Ong, et al., *Nature* **460**, 1101 (2009).
- [19] P. Roushan, J. Seo, C. V. Parker, Y. S. Hor, D. Hsieh, D. Qian, A. Richardella, M. Z. Hasan, R. J. Cava, and A. Yazdani, *Nature* **460**, 1106 (2009).
- [20] T. Zhang, P. Cheng, X. Chen, J. Jia, X. Ma, K. He, L. Wang, H. Zhang, X. Dai, Z. Fang, et al., *Phys. Rev. Lett.* **103**, 266803 (2009).
- [21] Y. Zhang, K. He, C. Chang, C. Song, L. Wang, X. Chen, J. Jia, Z. Fang, X. Dai, W. Shan, et al., arxiv: cond-mat/0911.3706 (2009).
- [22] P. Cheng, C. Song, T. Zhang, Y. Zhang, Y. Wang, J. Jia, J. Wang, Y. Wang, B. Zhu, X. Chen, et al., arxiv: cond-mat/1001.3220.
- [23] T. Hanaguri, K. Igarashi, M. Kawamura, H. Takagi, and T. Sasagawa, arxiv: cond-mat/1003.0100 (2010).
- [24] J. Chen, H. J. Qin, F. Yang, J. Liu, T. Guan, F. M. Qu, G. H. Zhang, J. R. Shi, X. C. Xie, C. L. Yang, et al., arxiv: cond-mat/1003.1534 (2010).
- [25] N. P. Butch, K. Kirshenbaum, P. Syers, A. B. Sushkov, G. S. Jenkins, H. D. Drew, and J. Paglione, arxiv: cond-mat/1003.2382 (2010).
- [26] D. Teweldebrhan, V. Goyal, and A. A. Balandin, *Nano Letters* **10**, 1209 (2010).
- [27] H. Steinberg, D. R. Gardner, Y. S. Lee, and P. Jarillo-Herrero, arxiv: cond-mat/1003.3137 (2010).
- [28] H. Tang, D. Liang, R. L. J. Qiu, and X. P. A. Gao, arxiv: cond-mat/1003.6099 (2010).
- [29] O. E. Ayala-Valenzuela, J. G. Analytis, J. Chu, M. M. Altarawneh, I. R. Fisher, and R. D. McDonald, arxiv: cond-mat/1004.2311 (2010).
- [30] Z. Alpichshev, J. G. Analytis, J. H. Chu, I. R. Fisher, and A. Kapitulnik, arxiv: cond-mat/1003.2233 (2010).
- [31] M. Koenig, H. Buhmann, L. W. Molenkamp, T. Hughes, C.-X. Liu, X.-L. Qi, and S.-C. Zhang, *J. Phys. Soc. Japan* **77**, 031007 (2008).
- [32] J. Linder, T. Yokoyama, and A. Sudb?, *Phys. Rev. B* **80**, 205401 (2009).
- [33] C. Liu, H. Zhang, B. Yan, X. Qi, T. Frauenheim, X. Dai, Z. Fang, and S. Zhang, *Phys. Rev. B* **81**, 041307 (2010).
- [34] H. Lu, W. Shan, W. Yao, Q. Niu, and S. Shen, *Phys. Rev. B* **81**, 115407 (2010).
- [35] L. Fu, *Phys. Rev. Lett.* **103**, 266801 (2009).
- [36] X.-L. Qi, T. L. Hughes, and S.-C. Zhang, *Phys. Rev. B* **78**, 195424 (2008).
- [37] X. Qi, R. Li, J. Zang, and S. Zhang, *Science* **323**, 1184 (2009).
- [38] W. Lee, C. Wu, D. P. Arovas, and S. Zhang, *Phys. Rev. B* **80**, 245439 (2009).
- [39] A. J. Mildred S. Dresselhaus, Gene Dresselhaus, *Group theory: application to the physics of condensed matter*, Springer, 2008.
- [40] R. Winkler, *Spin-orbit coupling effects in two-dimensional electron and hole systems*, Springer Tracts in Modern Physics, 2003.
- [41] W. Shan, H. Lu, and S. Shen, Arxiv:cond-mat/1001.0526 (2010).
- [42] B. Zhou, H. Lu, R. Chu, S. Shen, and Q. Niu, *Phys. Rev. Lett.* **101**, 246807 (2008).
- [43] H. Lu, W. Shan, W. Yao, Q. Niu, and S. Shen, arxiv: cond-mat/0908.3120 (2009).
- [44] Y. A. Bychkov and E. I. Rashba, *Journal of Physics C Solid State Physics* **17**, 6039 (1984).
- [45] W. Zhang, R. Yu, H. Zhang, X. Dai, and Z. Fang, arxiv: cond-mat/1003.5082 (2010).
- [46] H. Zhang, C. Liu, X. Qi, X. Deng, X. Dai, S. Zhang, and Z. Fang, *Phys. Rev. B* **80**, 085307 (2009).
- [47] J. M. Luttinger and W. Kohn, *Phys. Rev.* **97**, 869 (1955).
- [48] L. M. Roth, B. Lax, and S. Zwerdling, *Phys. Rev.* **114**, 90 (1959).

